Laboratory of Advanced Energy Systems
Department of Engineering Physics and Mathematics
Helsinki University of Technology
FIN-02015 HUT, Finland

TKK-F-A828

CURRENT DISTRIBUTION MEASUREMENTS AND MODELING OF MASS TRANSFER IN POLYMER ELECTROLYTE FUEL CELLS

Matti Noponen

Dissertation for the degree of Doctor of Science in Technology to be presented with due permission of the Department of Engineering Physics and Mathematics, Helsinki University of Technology for public examination and debate in Auditorium F1 at Helsinki University of Technology (Espoo, Finland) on the 26.03.2004, at 12 o'clock noon.

Distribution:
Helsinki University of Technology
Department of Engineering Physics and Mathematics
Laboratory of Advanced Energy Systems
P.O. Box 2200
FIN-02015 HUT
Finland
Tel. +358-9-451-3198
Fax +358-9-451-3195
http://lib.hut.fi/Diss/2004/isbn9512269783/

ISBN 951-22-6977-5 (printed)
ISBN 951-22-6978-3 (pdf)

ISSN 1456-3320 (printed)
ISSN 1459-7268 (pdf)

Otamedia Oy
Espoo 2004

PREFACE

The work presented in this dissertation has been carried out in three years between 2000 and 2003 at the Laboratory of Advanced Energy Systems at Helsinki University of Technology (HUT) and at the Laboratory of Applied Electrochemistry at Royal Institute of Technology (KTH). The work has been financed by the Nordic Energy Research (NEFP), which I would like to thank for the tremendously nice opportunity for the Nordic exchange.

I like to thank my supervisor Prof. Peter Lund from the Laboratory of Advanced Energy Systems for his guidance and support that he has provided during this thesis. I also express my deepest gratitude to Prof. Göran Lindbergh from the Laboratory of Applied Electrochemistry for giving me the chance to work under his supervision.

I would like to thank all of my colleagues for the pleasant working atmosphere both at HUT and KTH. Especially I own my gratitude for our fuel cell team at HUT: Mr. Tuomas Mennola, Mr. Tero Hottinen, Mr. Mikko Mikkola, Mr. Olli Himanen and Mr. Mikko Aronniemi. At least the same amount of gratitude is expressed to my co-workers at KTH: Dr. Anders Lundblad, Dr. Michael Vynnycky, Dr. Jari Ihonen and Dr. Erik Birgersson. Most probably, without Dr. Jari Ihonen, I would have had to live under a bridge during my stay in Sweden. I am also indebted to Mr. Michael Ross, a former member of our fuel cell group at HUT, for checking the language of this thesis.

Finally, I would like to thank my parents, Helena and Kari, my brother Sami and especially my forthcoming wife Hanna for the support and understanding you all have given me during this work.

Espoo, March 2004
Matti Noponen

ABSTRACT

The polymer electrolyte fuel cell (PEFC) is considered as an attractive option to produce electric power in many applications ranging from a few watt portable up to several kilowatt automotive applications. The advantage of the PEFC in these applications stems from its high efficiency, low emissions, silent operation and possible low production costs in the future. However, the main factor hindering the market penetration of PEFC applications is the present high production cost of the cell. To allow lower costs for the PEFC, the cell area has to be used efficiently in order to minimize the material usage. This requires the maximization of the cell performance by enhancing the current production at low potential losses.

At high current densities, mass transfer losses become the dominating loss mechanism. The mass transfer losses usually produce uneven current production throughout the active area of the cell. The local current production can be studied by experimental and computational methods. For the experimental characterization of the local current production, two different measurement system based on segmented current collectors have been constructed. The other is for a small PEFC operating with natural convection and the other is for a large PEFC operating with forced convection. In addition to the experimental methods, two different theoretical PEFC models have been developed, the other for the free-breathing PEFC and the other for the forced convection PEFC.

The current distribution studies were conducted for the free-breathing PEFC in order to determine the feasibility of using natural convection as an air supply method for the cathode reaction at different cell temperatures and ambient conditions. It was observed that the cell performance is highly dependent on the operating conditions and that the current distribution is uneven in the most cases.

The current distribution measurements conducted with the large PEFC were used mainly for the model validation purposes. It was shown that under certain operating conditions the current distribution was uniform and thus a one-dimensional PEFC model could be used. The results showed that two-phase and non-isothermal conditions are likely to exist when a PEFC is operated at high current densities and with well humidified gases.

TABLE OF CONTENTS

LIST OF PUBLICATIONS

A. M. Noponen, T. Mennola, M. Mikkola, T. Hottinen, and P. Lund, '*Measurement of current distribution in a free-breathing PEMFC*', Journal of Power Sources **106** (2002) 304-312.

B. M. Noponen, T. Hottinen, T. Mennola, M. Mikkola, and P. Lund, '*Determination of mass diffusion overpotential distribution with flow pulse method from current distribution measurements in a PEMFC*', Journal of Applied Electrochemistry **32** (2002) 1081-1089.

C. T. Hottinen, M. Noponen, T. Mennola, O. Himanen, M. Mikkola, and P. Lund, '*Effect of ambient conditions on performance and current distribution of a polymer electrolyte membrane fuel cell*', Journal of Applied Electrochemistry **33** (2003) 256-271.

D. T. Mennola, M. Noponen, M. Aronniemi, T. Hottinen, M. Mikkola, O. Himanen, and P. Lund, '*Mass transport in the cathode of a free-breathing polymer electrolyte membrane fuel cell*', Journal of Applied Electrochemistry **33** (2003) 979-987.

E. M. Noponen, J. Ihonen, A. Lundblad, and G. Lindbergh, '*Current distribution measurements in a PEFC with net flow geometry*', Journal of Applied Electrochemistry **34** (2004) 255-262.

F. M. Noponen, J. Ihonen, E. Birgersson, M. Vynnycky, A. Lundblad, and G. Lindbergh, '*A two-phase, non-isothermal PEFC model - theory and validation*', Submitted 30th of September 2003 to Fuel Cells - From Fundamentals to Systems.

BRIEF DESCRIPTION OF THE CONTENTS OF THE PUBLICATIONS

Publication A: A segmented current collector and measurement system for current distribution studies was introduced for a free-breathing PEFC. Local current distribution mapping at different cell temperatures was conducted. It was concluded that the cell performance is enhanced at elevated cell temperatures resulting in more even current distribution profiles.

Publication B: A highly over stoichiometric flow pulse was fed into the cathode channels of a free breathing PEFC. The current distribution, cell resistance and polarization were recorded simultaneously. From the difference between the flow pulse measurement and normal operation, an estimate could be made of the magnitude of different overpotentials affecting the current distribution.

Publication C: The effect of ambient conditions on the operation of a free-breathing PEFC was studied with climate chamber experiments using a segmented cell. From the results, the effect on cell performance of relative humidity and temperature gradient between the PEFC and the ambient air was determined. A temperature gradient is needed to enhance flow velocities, and extensive humidity causes severe mass transfer losses.

Publication D: A mass transfer model to describe flow velocity, and oxygen and water molar fractions for a free-breathing PEFC was introduced. The measured current distributions were used as boundary conditions at the cathode electrode to describe the cathode reaction rates. It was observed that the cell operated in a two-phase region when the temperature gradient was small between the PEFC and the ambient air. Furthermore, it was concluded that oxygen transport into the cathode by diffusion is small compared to the transport resulting from temperature differences.

Publication E: A segmented current collector and measurement system for current distribution studies was introduced for a forced convection PEFC. Local current distribution measurements were conducted with different stoichiometries, oxygen partial pressures, and humidity levels. It was shown that the differences in current distributions originating from mass transfer limitations and membrane resistance could be observed.

Publication F: A one-dimensional, multicomponent, two-phase and non-isothermal PEFC model was introduced. The model was validated with current distribution measurements, in which the local current production was even. A good agreement between measurements and the model was observed, and it was shown that a PEFC operated at high current densities is likely to operate under non-isothermal conditions.

AUTHOR'S CONTRIBUTION TO THE PUBLICATIONS

Publication A: The current distribution measurement system together with the segmented current collector plate was designed and largely constructed by the author. In addition, the author conducted the measurements. The article was written in close cooperation with all of the authors.

Publication B: The flow-pulse method was developed by the author. Measurements, analysis and most of the writing were conducted together with the co-authors.

Publication C: Author's contribution was in analyzing the results and the author also participated actively in the writing process.

Publications D: Author's contribution was in the model development, especially concerning the use of Maxwell-Stefan equation in the gas diffusion layer. The author also assisted in the analysis of the results and partook in the writing process.

Publication E: The current distribution measurement system together with the segmented current collector plate was mainly designed and constructed by the author. The analysis of the results and the writing were done together with the co-authors.

Publication F: The author contributed to the development of the model and the simulations. Results were analyzed and the article written together with the co-authors.

ABBREVIATIONS

a	Factor in Tafel equation
a_i	Activity of component i
A	Real catalyst area divided by geometric volume, m^{-1}
aq	Aqueous solution
B	Diffusion matrix, s m^{-2}
B_{ij}	Component in diffusion matrix, s m^{-2}
c	Concentration, mol m^{-3}
C_p	Heat capacity, J kg^{-1} K^{-1}
d	Driving force, m^{-1}
$Đ$	Maxwell-Stefan diffusivity, m^2 s^{-1}
$D^{(C)}$	Capillary diffusivity, m^2 s^{-1}
E	Potential, V
e	Normal vector
e^-	Electron
Eff	Effectiveness factor
$\mathcal{F}$	Faraday's constant, 96 485 A s mol^{-1}
F	External volumetric force, N m^{-3}
f	Factor in heat capacity
$F(s)$	Function of saturation
G	Gibbs free energy, J mol^{-1}
g	Gas
g	Acceleration of gravity, 9.81 m s^{-2}
H	Enthalpy, J mol^{-1}
h	Height, m
h_i	Enthalpy of component i, J mol^{-1}
I	Current, A
i	Current density, A cm^{-2}
i_0	Exchange current density, A m^{-2}
i_V	Volumetric current density, A m^{-3}
ℓ	Liquid
M	Molar mass, kg mol^{-1}
m	Mobility of the liquid phase
$\mathbf{n}_i$	Molar velocity of component i, mol s^{-1}
$\mathbf{N}_i$	Molar flux of component i, mol m^{-2} s^{-1}
p	Pressure, Pa
Pt	Platinum
q	Heat flux, W m^{-2}
R	Universal gas constant, 8.314 J K^{-1} mol^{-1}
S	Entropy, J K^{-1} mol^{-1}
s	Saturation
s_i	Entropy of component i, J K^{-1} mol^{-1}
T	Temperature, K
u	Velocity, m s^{-1}
v_i	Partial molar volume of component i, m^3 mol^{-1}
x	Molar fraction
ϰ	Stoichiometry
z	Electrons involved in electrochemical reaction
z	z-direction, m

Greek

α_c	Symmetry factor for cathodic reaction
Δ	Difference
ϕ	Potential, V
Φ	Relative humidity
γ	Porosity
γ_i	Activity coefficient of component i
η	Efficiency; Overpotential, V
φ	Surface tension, N m^{-1}
κ	Permeability, m^2
λ	Water content
μ	Dynamic viscosity, kg m^{-1} s^{-1}
μ_i	Chemical potential of species i, J mol^{-1}
θ	Wetting angle, rad
ρ	Density, kg m^{-3}
σ	Conductivity, S m^{-1}
ω	Volume fraction

Superscripts

0	Reference
c	Cathode
C	Capillary
m	Membrane
open	Open circuit
Pt	Platinum
Σ	Sum over all components

Subscripts

0	Reference
a	Anode
c	Cathode
diff	Diffusion, mass transfer, concentration
f	Sulfonic acid groups
H^+	Proton
H_2	Hydrogen
H_2O	Water
high	High heat value
i	Index for component
j	Index for component
k	Index for component
low	Low heat value
m	Membrane
n	Normal direction
n	Number of species
nucleus	Agglomerate nucleus
O_2	Oxygen
p	Hydraulic
polymer	Polymer in the electrode
pores	Pores in the electrode
rel	Relative
sat	Saturation
t	Total
z	z-direction
ϕ	Electrokinetic

1 INTRODUCTION

1.1 GENERAL

A fuel cell is an electrochemical energy conversion device that converts the chemical energy of fuel and oxidant directly into electricity and heat. A fuel cell is basically composed of an electrolyte and two electrodes, anode and cathode. Fuel is supplied to the anode where it is oxidized, i.e. electrons are liberated, and oxidant is supplied to the cathode where it is reduced. The electrolyte is an ionic conductive material that varies on the fuel cell type.

The fuel cell reaction was originally observed by Christian Schoenbein already in 1838 and Sir William Grove assembled the first fuel cell stack, constituting of 50 unit cells, in 1842 [1]. The term "fuel cell" was introduced by Ludwig Mond and Charles Langer in 1889 when they repeated Grove's earlier work [2]. They also introduced the porous electrode structure. The lack of understanding of the electrode kinetics, however, slowed the progress of fuel cells and the next breakthrough was not seen until 1932 when Francis T. Bacon introduced the first alkaline electrolyte fuel cell (AFC) using inexpensive nickel as the electrode material. His cell operated at 205 °C and 40 bars and the concept was demonstrated, e.g., in a tractor [2].

The U.S. National Aeronautics and Space Administration (NASA) became interested in the possibility of using fuel cells in space missions mainly because of technology's high gravimetric energy density (kWh kg^{-1}). They launched a major fuel cell program, which resulted e.g. in the development of a polymer electrolyte fuel cell (PEFC) in 1955 by William Grubb at General Electric (GE) [2]. This cell type is also known as a solid polymer fuel cell (SPFC) and proton (or ion-) exchange membrane fuel cell (PEMFC). The PEFC was the first fuel cell used in space missions, namely in the Gemini missions in 1962. AFCs were used in the later Apollo and Space Shuttle missions. Even though the fuel cells were successful in the space programs, the costs and various technical problems did not make them attractive for terrestrial applications.

Starting from the late 1960s until the middle 1980s, other fuel cell programs were launched, mainly in the U.S., aimed at developing an inexpensive fuel cell type for terrestrial markets. Fuel cells were seen as an attractive option because of their high efficiency, low emissions and the possibility of using various fuels, including coal. The phosphoric acid fuel cell (PAFC) was developed during these projects and was the only available commercial fuel cell type for many years [2-3].

The other two commonly known fuel cell types are the molten carbonate fuel cell (MCFC) and the solid oxide fuel cell (SOFC). Both fuel cell types operate at high temperatures: MCFC at 650 °C and SOFC between 600 and 1000 °C. MCFC was first introduced by Professor Baur in 1921 but he terminated the project because of corrosion and other material problems [2], still regarded as problematic in these cells today. The electrochemical reactions in a SOFC occur at an interface of only two phases (i.e. gas and solid) rather than the three phase interfaces of other fuel cell types, and thus it is regarded as one of the most promising fuel cell technologies. The first article on a SOFC was published in 1962 by a researcher from Westinghouse, a company that is still among the

leaders in SOFC technology [3]. Nowadays, MCFC and especially SOFC are considered attractive for large scale power and heat production.

Besides the SOFC, the most promising fuel cell type is the PEFC. After the Gemini program, two major developments enhanced PEFC development. These were the inventions of perfluorosulfonic-acid membranes and thin film electrodes. The new membranes provided longer lifetimes for the fuel cells because of the fully fluorinated structure. The thickness of such membranes has now been reduced to around ten micrometers, minimizing the performance losses. The thin film electrodes consist of a thin coating of electrolyte deposit on the electrocatalyst. This allows greater surface area and thus the expensive platinum catalyst loading can be significantly reduced compared to the conventional hot pressing process. The process was invented at the Los Alamos National Laboratory in the mid 1980s [3] and is still one of the most studied areas related to the PEFC.

PEFCs are seen as promising candidate for various applications ranging from small (i.e., a few watts) mobile applications up to automotive and power production applications of several kilowatts. For the low power applications, direct methanol fuel cells (DMFC) are usually the most attractive alternative among the fuel cells because they uses methanol for fuel instead of hydrogen. Methanol, a liquid at room temperature, has higher gravimetric energy density than hydrogen stored in pressure or metal hydride vessels. A DMFC is, from a structural point of view, similar to a PEFC but it has more severe problems with electrode poisoning, current losses due to methanol crossover and flooding. The first small fuel cell powered applications are on their way to markets; see e.g. [4].

Automotive applications, including passenger cars, buses and trucks, are nowadays the main driving force in the development of PEFCs. These applications may be the most challenging, however, mainly because of strict cost targets and lack of service networks. A system cost around 50 € kW^{-1} is seen acceptable but the present cost of a PEFC is still much higher. In addition, commercialization is still hindered by technical problems including e.g. long start-up times (especially in cold climates), cell temperature control in hot climates and lack of fuel storage techniques enabling high energy densities.

PEFCs are also considered as attractive for small scale combined heat and power production (CHP). The disadvantage of a PEFC in a CHP application is its low operating temperature. The temperature is not enough to produce industrial steam and the range of possible fuels are limited because of electrode poisoning. Therefore possible PEFC-CHP applications are usually limited to households at locations where natural or city gas is already available. The cost requirement for a household-sized PEFC stack is about 500 € kW^{-1} and the system should last up to 40,000 hours, a particularly difficult requirement.

1.2 MOTIVATION

Optimization of the efficiency of a PEFC system is a complicated task involving not only maximization of the PEFC efficiency but also minimization of the parasitic losses caused by the auxiliary system components. These may include compressors delivering and pressurizing reactant gases, pre-humidification systems to enhance hydration and thus proton conductivity of the ion-conductive phases, and pumps or fans for temperature control system all of which usually require energy.

Small PEFC applications are attractive when the weight of the storage is not the most critical aspect of the system but reliability and high efficiency are required. Hydrogen can be stored in metal hydrides that have high volumetric energy density and oxygen can be taken directly from the surrounding air. For small systems, the volumetric energy density can be critical, and thus every auxiliary component in the system, such as pre-humidifiers, mass flow controllers, compressors and temperature regulators, potentially decreases the density. Therefore it can be attractive for a PEFC in such systems to operate passively, including free convection (i.e. natural convection) to deliver oxygen for the cathode reaction and the use of dry hydrogen.

The use of free convection potentially increases the mass transfer losses due to unregulated stoichiometry, which may result in diluted oxygen concentrations and even severe flooding. The use of dry hydrogen may result in increased membrane resistance and even distorted resistance profiles. The ambient conditions, i.e. temperature and relative humidity, may also affect the cell performance, but a small PEFC system should be able to work in various ambient conditions. Therefore it is important to study cell performance in these conditions with methods that enable the determination of the system and PEFC feasibility compared to other options.

Most commonly air is, however, fed by forced convection into the cathode of a PEFC to enhance mass transfer, and pre-humidification is used to enhance hydration and thus conductivity of the ion-conducting materials. Cell temperature is increased to around 80 °C, up to the maximum temperature at which membrane degradation rate is still fairly low, to enhance electrochemical activity of the catalyst. Gases may also be pressurized to further enhance the mass transfer and electrochemical activity.

Mass transfer limitations are always emphasized at high current densities even if forced convection is used because product water has to be transported from the cell in order to prevent it from flooding. At high current densities, cell cooling to remove heat produced in the reaction becomes important. For example, if the cell is operated at a 1 A cm^{-2} current density and a potential of 0.5 V, the heat production can be almost 1 W cm^{-2}. Some of this heat can be used to vaporize the product water but most of it has to be transported from the cell to prevent it from overheating. Such high heat rejection rates can also produce significant temperature gradients inside a PEFC if some of the cell components have low thermal conductivity.

The optimization of PEFC geometry usually requires the minimization of the mass transfer losses at conditions where liquid water is likely to exist. Both computational and experimental tools can be used for optimization. With the computational approaches, different geometrical options can be studied with reasonable costs and time limits. Experimental approaches, especially those enabling mapping of local cell phenomena, are required to validate different computational models.

1.3 OBJECTIVE AND APPROACHES

The aim of this thesis is to provide reasonable measurement and computational techniques for analyzing local mass transfer phenomena occurring in a PEFC. Two different current distribution measurement systems using segmented current collectors have been constructed, one for a free-breathing PEFC and the other for a forced convection PEFC. In addition, two different computational PEFC models have been developed in order to enable studies of local cell phenomena other than current. These include airflow velocities and concentration profiles in the gaseous phase for free-breathing PEFCs, and velocities, pressure drops, concentrations, temperature, and voltage profiles in the gaseous and liquid phases for forced convection PEFCs.

The feasibility of using natural convection to supply oxygen for the cathode reaction is studied with the current distribution measurements at different cell and ambient conditions. The cell geometry was chosen to be straight channels open to the ambient air at the cathode side. The channel geometry facilitates modeling and thus reduces the complexity of the model and the calculation time and memory requirements. A commercial finite element method solver, FEMLAB®, was chosen for the simulations since the model is highly nonlinear and must be solved numerically as a result.

The current distribution measurements for the forced convection PEFC were mainly used for model validation purposes but also two different cell geometry options were studied experimentally. The use of current distribution measurements enables the validation of models ranging from one to three dimensions. The segmented current collector did not have channels but rather a mesh was used for the flow medium. The use of the mesh should allow one dimensional current distributions at high stoichiometries and reasonable humidification levels. The geometry studied during this thesis was restricted to one dimension, again in order to allow model simplifications, reduced calculation times and lower memory requirements for the computer. The same commercial FEM solver was used for simulations as in the case of the free-breathing PEFC.

The PEFC models used in this thesis lack a proper treatment of the transfer processes occurring in the membrane. Therefore a literature study on the subject was conducted as a part of the introduction. No good explanation of the assumptions of the different models was found from the references and thus they are here explained and justified based on a model derived by the author. In addition, the reversible PEFC potential and efficiency are calculated at different cell conditions in order to show that even these can have a distributed nature in a working PEFC.

2 POLYMER ELECTROLYTE FUEL CELL

2.1 FUEL CELL COMPONENTS

A polymer electrolyte fuel cell (PEFC) is an electrochemical energy conversion device. Like any other electrochemical reactor, a fuel cell contains an electrolyte and two electrodes, namely anode and cathode. In the case of a PEFC, hydrogen is used as a fuel at the anode side where it is oxidized into protons. Protons are transferred through the electrolyte and electrons via an external electric circuit to the cathode where oxygen is reduced. For the mass transfer processes, gas diffusion layers and bipolar plates are required to deliver reactants on the electrode surfaces. The structure of a PEFC unit cell is illustrated in Figure 1.

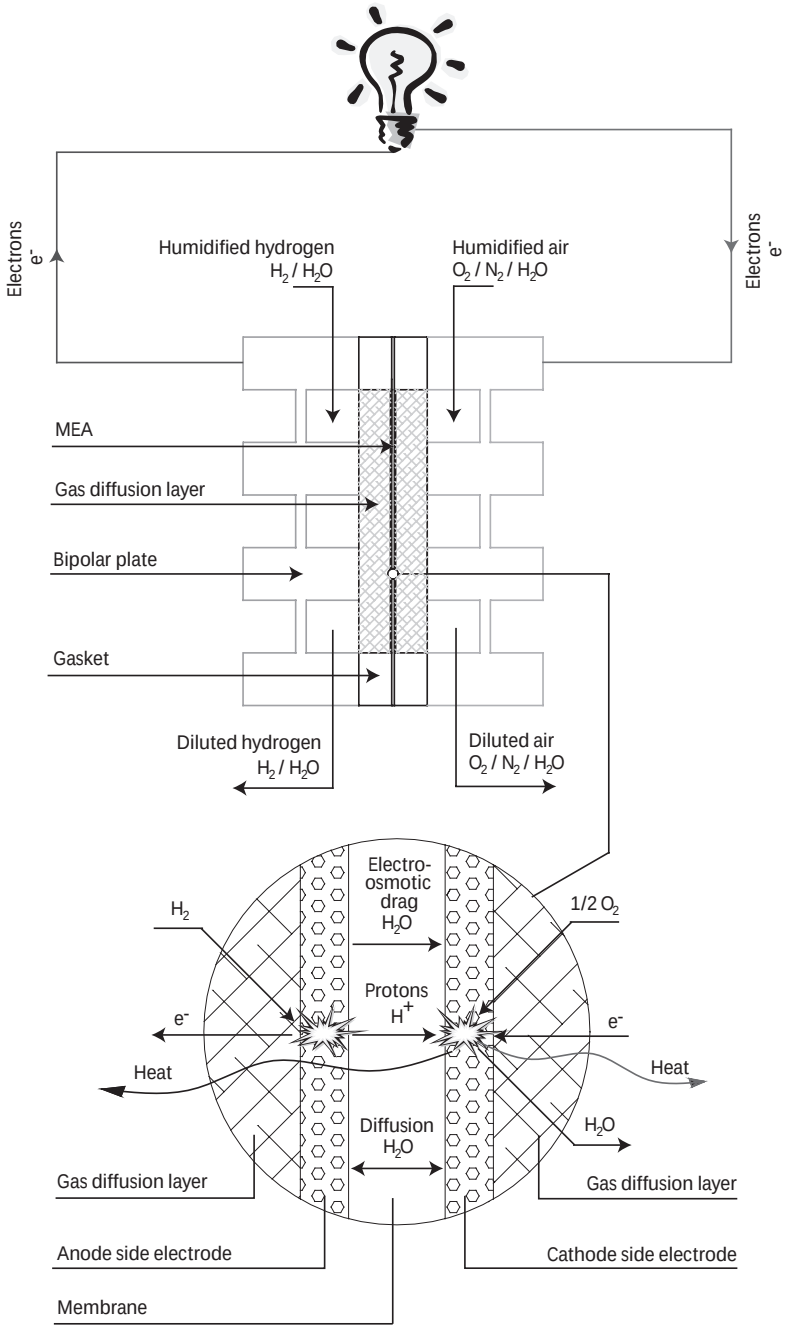

Figure 1. Structure of a PEFC with schematic mass and energy balances

2.1.1 MEMBRANE

The electrolytes used in PEFCs are solid polymer membrane structures. The most commonly used electrolyte material is Nafion® (E.I. duPont de Nemours and Company). Nafion® is a perfluorosulfonic acid (PFSA) polymer, a perfluorosulfonic acid / polytetraflouethylene (PTFE) copolymer in the acid (H^+) form [5]. PTFE forms a hydrophobic backbone on which the highly hydrophilic sulfonic acid groups are ionically bonded. Other similar PFSA membranes have been manufactured by Dow Chemical (Dow XUS®), Gore (Gore-Select®) [6], Ballard (BAM®) [7], Asahi Chemical Industry Co. (Aciplex®-S) and Asahi Glass Company (Flemion®). The chemical structure of some of these membranes is illustrated in Figure 2

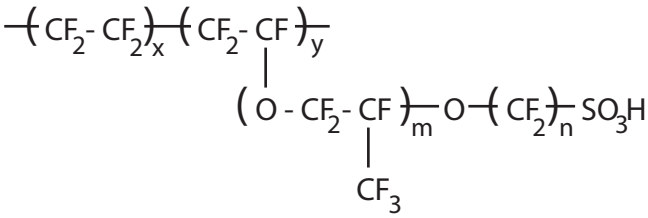

Figure 2. Chemical structure of Nafion®, Flemion, Aciplex, and Dow membrane [8], where:

Nafion®117: $m \geq 1$; $n = 2$; $x = 5 – 13.5$; $y = 1000$
Flemion®: $m = 0, 1$; $n=1\text{-}5$
Aciplex®: $m = 0, 3$; $n = 2 – 5$; $x = 1.5 – 14$
Dow XUS®: $m = 0$; $n = 2$; $x = 3.6 – 10$

The advantages of PFSA membranes are their high mechanical and chemical strength, and ability to enhance high proton conduction when they are hydrated. Furthermore, the manufacturing price of these materials should meet the cost targets assigned for fuel cell applications [9].

Because the proton conductivity of these membranes is highly dependent on the hydration level, one of the most important research fields regarding PEFCs has been effective water management of the cell. At low hydration levels, conductivity of the membrane decreases drastically, and at high hydration levels liquid, water saturation decreases the mass transport of the reactants to the electrode.

The operating temperature of these membranes is usually limited to between 0 and 100 °C. It might, however, be beneficial to operate PEFCs at higher temperatures in automotive or CHP applications. Recently phosphoric acid doped polybenzimidazole (PBI-H_3PO_4) membranes have shown promising performance at elevated temperatures [10]. Other types of membranes based on different polymers and charge carriers have also been investigated at elevated temperatures. A comprehensive review of different proton conductive polymers at high temperatures has been prepared by Jannasch [11].

2.1.2 ELECTRODES

The membrane is sandwiched between two electrodes, the anode and cathode. At the anode, hydrogen is oxidized and at the cathode oxygen is reduced, forming water on a catalyst surface. In order to enable the reaction, the catalyst surface must have access to proton conductive, electron conductive and gas phases, i.e. a three phase boundary structure. Therefore, PEFC electrodes are porous structures consisting of proton conductive polymer and supported catalyst.

A porous structure is required to enable the passage of reactants to the catalyst surface and also to maximize the active area, where reactions can occur. The proton conductive polymer has to be compatible with the membrane in order to minimize contact losses and to enhance good mechanical and chemical properties for the junction. Nafion® is usually used for this purpose. Carbon supported platinum is used as the catalyst material for the electrodes if pure reactants are used. If the anode gas stream contains impurities such as carbon monoxide, a mixture of platinum and ruthenium is often used. Carbon is used as a supporting material because it does not react with noble metals at fuel cell conditions and it provides sufficient electron conductivity. Carbon supported platinum is in an agglomerated form when used in a PEFC as has been shown computationally e.g. by Boyer et al. [12], Bultel et al. [13-14] and Jaouen et al. [15-16].

Electrodes are usually fabricated directly on the membrane e.g. by spraying or screen printing a solution made of proton conductive polymer catalyst ink. This type of structure is called a membrane electrode assembly (MEA). Electrodes are usually thin, only some tenths of micrometers and platinum loading is in a range of 0.3 mg_{Pt} cm^{-2} per side when pure hydrogen is used.

2.1.3 GAS DIFFUSION LAYERS

Gas diffusion layers have to permit homogenous transfer of reactants to and water away from the electrodes, as well as have appropriate electric conductivity, heat conduction and mechanical properties. The rate of fuel cell reactions, i.e. the current density, is directly proportional to the concentration of oxygen and hydrogen. Thus it is important that the concentration of the reactants throughout the electrode be as high and homogenous as possible in order to enable maximal current production. In addition, both liquid and gaseous water has to be transferred from the electrodes in order to prevent them from blocking the passage of reactants to the catalyst surface and from diluting the concentration of reactants. Furthermore, firm contact between the gas diffusion layer and the electrode surface has to be maintained to ensure good electrical and thermal conductivity properties for interfaces, and mechanical support for a flexible MEA.

Gas diffusion layers are usually made of highly porous carbon cloth or carbon paper, which is treated with hydrophobic resin, usually Teflon®. The porous structure enables sufficient mass transfer for the gaseous species whereas the hydrophilic resin is used to enhance liquid water transfer. Carbon is again chosen because of its conductive and durability in PEFC operating conditions. Despite the many critical functions of the gas diffusion layers, only a few experimental

studies have been reported on the subject. There are still many unknown properties of these materials, especially those concerning liquid water transfer and mechanical stiffness under compression.

2.1.4 BIPOLAR PLATES

A flow field and separator plate is usually one integrated component of a PEFC. A cooling plate can also be integrated into this structure. Flow fields are required to deliver reactants throughout the active cell area and to transport reaction products so that they do not dilute the concentration of reactants. Separator plates are needed when the unit cells are piled into a stack in order to ensure that no mixing of reactants occurs and in order to connect unit cells electrically in series, so as to increase the voltage of the PEFC. The integrated structure of a flow field and separator plate (and cooling plate) is called a bipolar plate. The material used is usually graphite, steel or composite carbon, and plates are manufactured either by machining, stamping or molding processes.

Graphite has generally been used in laboratory cells but its manufacturing process is regarded as too expensive for serial production. Different steel types have also been tested as bipolar plate materials for a PEFC, see e.g. Wang et al. [17]. The advantages of steel structures are their mechanical strength enabling very thin structures and low cost. Disadvantages are usually high contact resistances and corrosion. Both of these can be improved by protective coatings such as gold [18] or carbon [19]. Composite bipolar plates are usually made of carbon-polymer composite [20] but carbon-carbon composites [21] have also been investigated. The major advantage of composite-carbon bipolar plates is their low cost in serial production. However, there is always a trade-off between mechanical strength and conductivity with these materials [19].

The usual geometries used for flow fields are parallel, serpentine, combination of parallel and serpentine, interdigitated and net. The main requirement for an effective flow field is that it ensures a homogenous concentration profile for reactants throughout the active cell area. Thus, there are generally three optimization tasks for the geometry, i.e. low and equal pressure drop for gases in each channel, effective liquid water removal characteristics, and channel-rib ratio.

Low pressure drop ensures high gas velocities in the channels at low energy consumption rates of pumps or compressors needed to generate forced convection. Pressure drop establishes constraints for the ratio of channel length and cross-sectional area of the channel. Equal pressure drop in parallel channels is required to ensure equal velocity profiles and thus equal concentrations for reactants. Effective liquid water removal from the channels can be attained with sufficient gas flow velocities and geometry options. Since liquid water is usually attached to channel walls, these surfaces can be polished or treated with some hydrophobic agent in order to improve the liquid flow mechanism. Serpentine flow geometry, for example, enhances water removal because gas flow drags all droplets with it. Some of the channels in parallel channel geometry may get flooded and gas flow in these channels is weakened. The optimization of the channel-rib ratio involves

minimization of reactant dilution, minimization of resistive losses and maximization of mechanical support for the gas diffusion layers, and thus the optimum value depends strongly on the material properties of the gas diffusion layer.

A PEFC usually requires a cooling unit in order to prevent it from overheating. The heat transfer medium is typically air or liquid water. The requirement for cooling power is determined by the geometrical size, materials used in the cell and power density. If the PEFC is operated at low power densities and the product heat energy is not utilized, air cooling is usually sufficient. However, when high power densities or heat utilization are desired, water (or other liquid) cooling is used. In that case, a cooling plate is required typically after each unit cell. Flow geometries used for the heat transfer medium are similar to those used for anode and cathode flow fields.

2.1.5 OTHER CELL COMPONENTS

A PEFC requires other types of components and structures, such as gaskets, endplates, clamps and gas manifolds. Gaskets are usually made of some nonconductive polymer such as Teflon or silicon rubber. They have to be impermeable for gases and have sufficient corrosion resistance. Endplates are used to mechanically support the fuel cell. It has been found out that the clamping pressure on the active area of a unit cell should be around 10 bar [22], and thus the endplates have to endure fairly high mechanical forces. Traditionally endplates are made to be thick to overcome the bending problems. However, advanced structures such as the so-called 'Dbow-concept' may decrease the material needed, and thus the weight and volume of the endplates [23].

In addition to the PEFC components, a variety of auxiliary components such as temperature controllers, mass flow regulators, gas humidifiers, compressors and gas purification systems are required to operate a PEFC. An example of a PEFC system, used for back-up power in telecommunication application, is presented by Varkaraki et al. [24]. Even though the auxiliary devices usually improve the performance of a PEFC, they simultaneously decrease the total efficiency of the system, i.e. additional power is required to operate the auxiliary components, and thus the PEFC has to be oversized to power them as well as the load. Especially in the case of low power applications, the power consumption of the auxiliary devices has to be minimized. Therefore solutions allowing passive operation and control may be desirable. Even though the passive methods may lead to decreased cell performance, they may at the same time offer higher efficiencies for the system as a whole.

2.2 REVERSIBLE PERFORMANCE OF THE PEFC

The theoretical efficiency and cell potential defines the maximum available power for any kind of electrochemical process producing energy. Even though the subject is well studied and understood for different electrochemical reactions, the author is not aware of studies in which it is shown that the theoretical fuel cell potential and efficiency can vary throughout the active area. Therefore, a study is presented hare, based on the earlier work carried out by Lampinen and Fomino [25] with the exception that the stoichiometry and reactant gas humidities are included.

The half cell reaction for the anode is given in Equation (1), the half cell reaction for the cathode in Equation (2) and the total reaction in Equation (3). Reaction enthalpies (ΔH), entropies (ΔS) and reversible potentials (E_i) occurring on the platinum surface are given for conditions of 25 °C and 1 bar. Values are taken from [25].

$$\mathrm{H_2(g) \rightarrow 2H^+(aq) + 2e^-(Pt_a)} \qquad \begin{aligned} \Delta H^{\mathrm{Pt}} &= 2829.0\,\mathrm{kJ\,mol^{-1}} \\ \Delta S^{\mathrm{Pt}} &= 0.104\,\mathrm{J\,mol^{-1}\,K^{-1}} \\ E_a^{\mathrm{Pt}} &= 14.66\,\mathrm{V} \end{aligned} \qquad (1)$$

$$\mathrm{O_2(g) + 4H^+(aq) + 4e^-(Pt_c) \rightarrow 2H_2O(\ell)} \qquad \begin{aligned} \Delta H^{\mathrm{Pt}} &= -6229.6\,\mathrm{kJ\,mol^{-1}} \\ \Delta S^{\mathrm{Pt}} &= -326.36\,\mathrm{J\,mol^{-1}\,K^{-1}} \\ E_c^{\mathrm{Pt}} &= 15.88\,\mathrm{V} \end{aligned} \qquad (2)$$

$$\mathrm{H_2(g) + \tfrac{1}{2}O_2(g) \rightarrow H_2O(\ell)} \qquad \begin{aligned} \Delta H^{\mathrm{Pt}} &= -285.8\,\mathrm{kJ\,mol^{-1}} \\ \Delta S^{\mathrm{Pt}} &= -163.08\,\mathrm{J\,mol^{-1}\,K^{-1}} \\ E &= 1.23\,\mathrm{V} \end{aligned} \qquad (3)$$

It should be noted that the half cell enthalpy, entropy and potential values do arise out of a one-phase contact between platinum and gaseous reactants. In reality, these values are somewhat different because the platinum particles are also in contact with the proton and electron conductors.

In the calculation conducted by Lampinen and Fomino [25], only one temperature level was used, a temperature at which all water is produced as liquid in the cathode reaction. In addition, it was assumed that pure reactants are used in the fuel cell reactions. There are, however, two interesting composition possibilities for the cathode side, i.e. humidified oxygen and humidified air. At the anode side, compositions can vary to a great extent more if reformate gases are used. However, only the humidified hydrogen is regarded here. The relative humidity can vary between 0-100 % in PEFC applications and the stoichiometry, at least in theory, from one to infinity.

The theoretical fuel cell potential (i.e., the reversible cell potential) is defined as the maximum chemical energy available for electric work divided by the electric charge transferred in the process. It can be shown (see e.g. Koryta et al. [26]) from the first and the second law of thermodynamics that the theoretical potential of a fuel cell using hydrogen and oxygen is equal to:

$$E(T,p) = -\frac{\Delta H(T,p) - T\Delta S(T,p)}{z\mathcal{F}} = -\frac{\Delta G(T,p)}{z\mathcal{F}}$$
$$= -\frac{\Delta G_0(T)}{z\mathcal{F}} - \frac{\mathrm{R}T}{z\mathcal{F}} \ln\left(\frac{a_{\mathrm{H_2O}}(T,p,x_{\mathrm{H_2O}},x_{\mathrm{O_2}})}{a_{\mathrm{H_2}}(T,p,x_{\mathrm{H_2}}) a_{\mathrm{O_2}}(T,p,x_{\mathrm{H_2O}},x_{\mathrm{O_2}})^{1/2}} \right) \quad (4)$$

The Gibbs free energy (ΔG) is a function of temperature (T), pressure (p), and composition of the reactants and products (x_i) and this dependency is often described by the activity of the species (a_i). In a conventional PEFC, the operating temperature is under 100 °C and thus the produced water can be theoretically formed either as liquid or gas. The activity of liquid water is usually approximated as unity, and the activity of gaseous species is determined by their molar fractions. Derivation of the theoretical fuel cell potential as a function of temperature, pressure, and composition of reactants and products is shown in Appendix A.

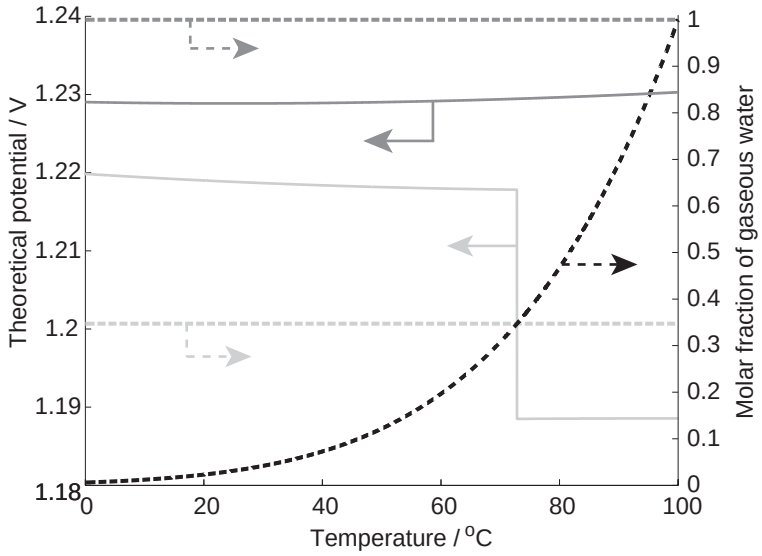

Figure 3. Theoretical fuel cell potential (solid line) and molar fraction of water vapor in product gases (dashed line) as a function of temperature for oxygen (▬) and air (▬). The maximum molar fraction of vapor in air is marked with black dashed line. Relative humidity and stoichiometry for inlet gases is 0 % and 1, respectively. Total pressure is 1 bar.

The theoretical fuel cell potential with unit stoichiometry and relative humidity of zero is depicted Figure 3. It can be seen that with pure oxygen the temperature dependency is negligible because the water is produced as liquid throughout the temperature range and the temperature dependency of the reaction's Gibbs free energy is minor. On the other hand, the reversible cell potential changes radically as a function of temperature when air is used. At about 70 °C, water starts to be produced in gaseous form. This can be observed from the difference in maximum molar fraction of vapor in air and the molar fraction of vapor in product gas. If the vapor pressure in product gas is lower than the maximum possible vapor pressure, water is produced in gaseous form. However, if the maximum possible vapor pressure is obtained, the excess water is condensed and the vapor pressure

in the product gas stream is the saturation pressure in air at the given conditions. The drop in the reversible potential is caused by the change in the Gibbs free energy when vaporization of water occurs.

The effect of the relative humidity and stoichiometry on the theoretical potential is depicted in Figures 4 and 5, respectively. Stoichiometry is set to one in Figure 4 and relative humidity to zero in Figure 5. The same relative humidity and stoichiometry is used for the anode and cathode side in both Figures. The pressure at the electrodes is 1 bar in both cases.

The reversible potential is considerably changed at elevated temperatures and high humidity levels because water vapor decreases the molar fraction of oxygen, both with pure oxygen and air, as seen from Figure 4. At 100 °C and 100 % relative humidity, only gaseous water is present and the reversible potential becomes zero because no reactants are present in the inlet gas streams.

Differences in stoichiometry affect the reversible cell potential because at elevated stoichiometries the water removal from the reaction surfaces becomes more effective, as seen from Figure 5. Thus, the water produced in the reaction becomes gaseous at lower temperatures. When the stoichiometry is further increased, the molar fraction of water is simultaneously decreased in the outlet gas stream, and thus the reversible cell potential is increased.

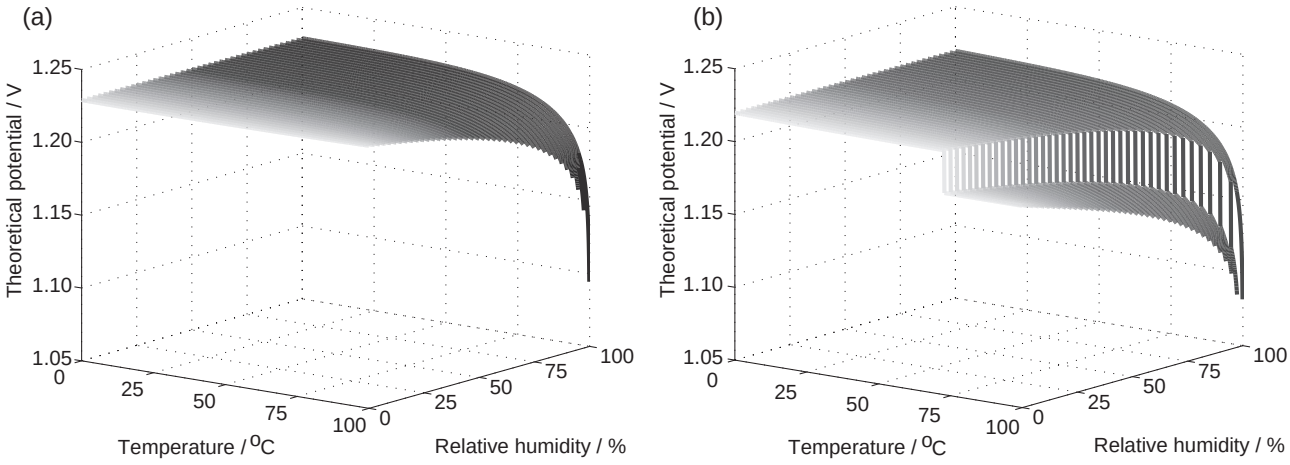

Figure 4. Theoretical fuel cell potential as a function of temperature and relative humidity for oxygen (a) and air (b). Stoichiometry is 1 and total pressure 1 bar.

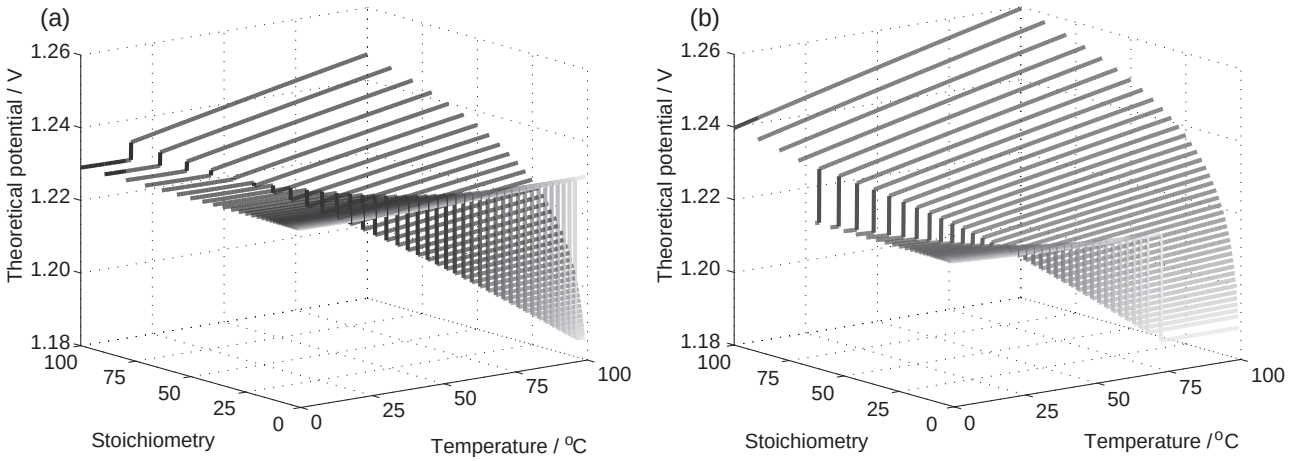

Figure 5. Theoretical fuel cell potential as a function of temperature and stoichiometry for oxygen (a) and air (b). Relative humidity of the inlet gases is zero and total pressure 1 bar.

The efficiency of a fuel cell or a fuel cell system affects the competitiveness of the system compared to alternatives power sources. Efficiency is defined as the ratio of the energy obtained from the process to the energy put into the process. In the case of a fuel cell, electric efficiency is expressed as:

$$\begin{aligned}\eta_{\mathrm{FC,el}} &= \frac{\text{Electric energy from the fuel cell}}{\text{Energy into the fuel cell}} \\ &= \frac{EI}{-\Delta H \mathbf{n}_{\mathrm{H_2}}} \\ &= \left(\frac{-\Delta G}{-\Delta H}\right)\left(\frac{E}{-\Delta G/2\mathcal{F}}\right)\left(\frac{I}{2\mathcal{F}\mathbf{n}_{\mathrm{H_2}}}\right) \\ &= \eta_{\mathrm{reversible}}\eta_{\mathrm{voltage}}\eta_{\mathrm{current}}\end{aligned} \tag{5}$$

It can be seen from Equation (5) that the electric efficiency is a function of the transformation of the chemical energy of the fuel into electric energy, $\eta_{\mathrm{reversible}}$, voltage divided by the theoretical voltage, η_{voltage}, and current divided by the theoretical current, η_{current}. The reversible efficiency is a function of temperature, pressure, and composition of the reactants and products, as with the reversible cell potential. At room temperature, ambient pressure, and unit stoichiometry, the reversible fuel cell efficiency is about 0.83, i.e. 83 % of the chemical energy of the fuel can be transformed into electricity by the fuel cell reaction (3). The reversible fuel cell efficiency was also studied here as a function of temperature, relative humidity and stoichiometry at the same conditions as were studied for reversible potentials. The derivation is shown in Appendix B.

Figure 6 depicts the situation where stoichiometry is set to one but relative humidity and cell temperature are changed. The most pronounced changes in the reversible fuel cell efficiency occur at the same conditions as the major changes in the reversible potential. No severe decrease in

reversible efficiency is noticed when oxygen is used at low and moderate temperatures and relative humidity levels. However, when air is used a notable change is observed when water starts to be produced as gas. Although both the Gibbs free energy and enthalpy change as a function of temperature, the change in the Gibbs free energy is more significant and thus an upward step function is observed.

The situation where relative humidity is set to zero but stoichiometry and temperature are changed is depicted in Figure 7. Increases in stoichiometry increase the reversible fuel cell efficiency because water is again produced in gaseous form. It is interesting to see that the reversible efficiency can be over one. It should, however, be noticed that the current efficiency, which is the inverse of the stoichiometry, is not included in this study. If that is included in theoretical efficiency, fuel cell efficiency starts to decrease at elevated stoichiometries.

The reversible potential and efficiency are shown to depend on the cell temperature, stoichiometry and humidity. Therefore, the reversible potential and efficiency of a fuel cell, in which the temperature and the concentration of reactants are not uniform throughout the cell, obtain different values in different cell locations.

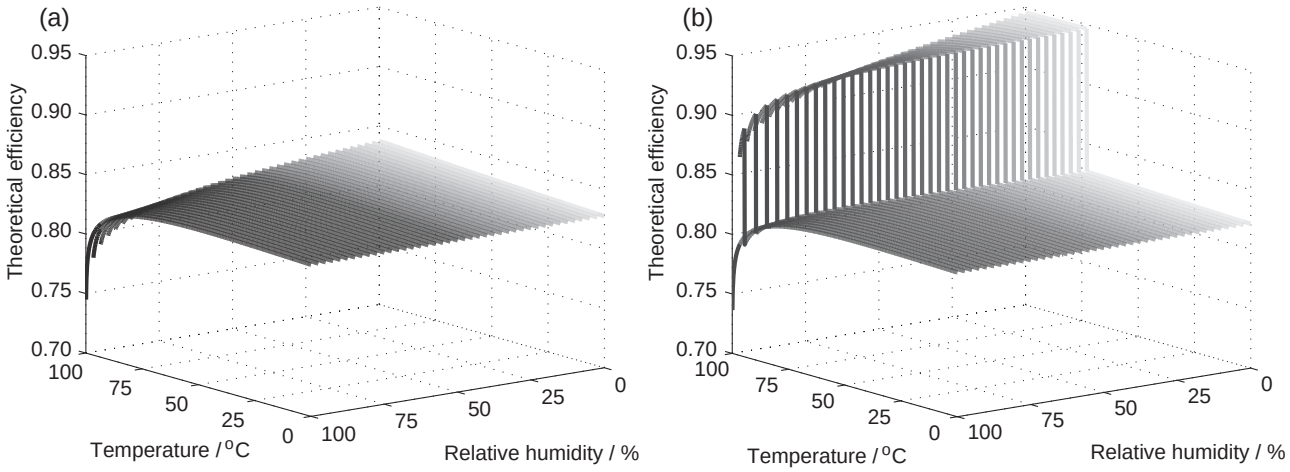

Figure 6. Theoretical fuel cell efficiency as a function of temperature and relative humidity for oxygen (a) and air (b). Stoichiometry is 1 and total pressure 1 bar.

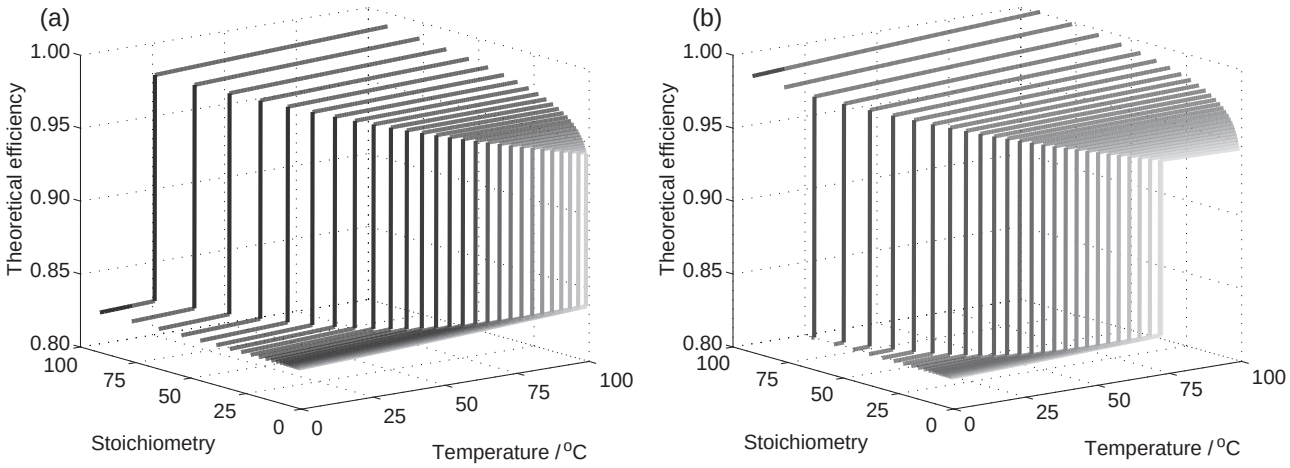

Figure 7. Theoretical fuel cell efficiency as a function of temperature and stoichiometry for oxygen (a) and air (b). Relative humidity of the inlet gases is zero and total pressure 1 bar.

The voltage efficiency is usually the most significant single source reducing the total efficiency. While the reversible cell potential is around 1.2 V at normal operating conditions, the real cell voltage when current is taken from the cell is around 0.6 V, thus giving a voltage efficiency of 0.5. More detailed discussion on the different factors resulting in voltage losses in a PEFC are discussed in Section 2.3. The current efficiency can be close to one in well-designed systems. The fuel cell is usually operated at the anode side with stoichiometric levels higher than one, but the non-reacted hydrogen can be circulated back to the inlet, e.g. with a pump. Some of the hydrogen is always leaked through the membrane but can be shown to be minor, e.g., by Dannenberg and Ekdunge [27].

2.3 ACTUAL PERFORMANCE OF THE PEFC

2.3.1 OPEN CIRCUIT POTENTIAL

The open circuit voltage of a real PEFC is always lower than the reversible cell potential. This is mainly caused by three factors, which are activation potential of the half cell reactions, impurities on the catalyst surfaces, and side reactions.

Parathasarthy et al. [28] concluded that the low exchange current density of the oxygen reduction reaction, i.e. the high activation energy required for reduction of oxygen, contributes to the decrease in potential. The exchange current density at the anode side is 5 to 6 orders of magnitude higher than the cathode side, and thus its effect on the open circuit potential should be minor.

Bockris and Srinivasan [29] concluded that the main cause of lowered open circuit potential is impurities that cause oxidation reactions at the cathode. Possible impurities include all species that react electrochemically on platinum surfaces at the operating conditions of a PEFC, even including

hydrogen that has diffused from the anode. Damjanovic et al. [30-31] found out that the oxygen reduction reaction on a platinum surface involves three- or four-step mechanism including the possibility of peroxide production, which again may cause mixed potentials reducing the open circuit potential.

The drop at open circuit conditions has already a significant impact on the efficiency of a PEFC. A typical value for an open circuit potential is 1 V, and the corresponding drop in voltage efficiency is approx. 15 %.

2.3.2 CURRENT-VOLTAGE BEHAVIOR

Figure 8 illustrates a typical current-voltage, i.e. polarization, curve for a PEFC and Figure 9 a typical potential profile in a normal direction, i.e. through the cell, for a one dimensional PEFC at a given current density. The polarization curve can be divided into three regions in which different phenomena limit the cell performance. At low current densities, the activation energy required to maintain cathode side half reaction is the main limiting phenomenon (Region I in Figure 8). In the middle region (Region II), ohmic losses occurring mainly in the membrane dominate, and when the current density is further increased, mass transfer losses, i.e. reduced oxygen molar fraction at the cathode electrode, become significant (Region III). These limiting phenomena are usually called overpotentials, i.e. the activation, ohmic and mass transfer overpotential.

The potential profile in Figure 9 gives an approximation of the losses due to different components. The most significant losses occur at the cathode side electrode, due to the high activation energy required for the oxygen reduction reaction, and mass transfer losses, caused by reduced oxygen molar fraction. The second biggest losses occur usually in the membrane because of its relatively low ionic conductivity. The anode side activation losses are usually of minor importance if pure hydrogen is used. If reformate gas is fed to the anode, the overpotential can be much higher. The ohmic losses in the gas diffusion layers and bipolar plates are usually also lower than the cathode side activation and membrane ohmic overpotentials. Losses occurring at the cathode electrode and membrane are discussed more thoroughly in the next subchapters. The overall cell potential is obtained by subtracting the anode side terminal voltage, i.e. the voltage at the left-hand side, from the cathode side terminal voltage, i.e. the voltage at the right-hand side.

There is no definition for where one limiting region starts and the other ends but mathematically these can be characterized as a logarithmic (Region I), linear (Region II) and exponential [32] or logarithmic [33] (Region III) parts. However, the real polarization of a PEFC is a much more complicated modeling task. An accurate PEFC model would draw on a variety of engineering disciplines, ranging from material science to electrochemistry and fluid dynamics. Some of these are covered in the next subchapters.

Figure 8 also depicts a normal current-power characteristic curve for a PEFC. Usually power density rises with current density until a maximum is reached at high current densities, beyond

which the mass transfer limitations start to reduce the power density. For a PEFC system, a typical desirable operating range hence lies in the region up to the maximum power density. The determination of an optimal operation point using only a polarization curve is, however, much more difficult, and is also affected by economic and other application specific parameters.

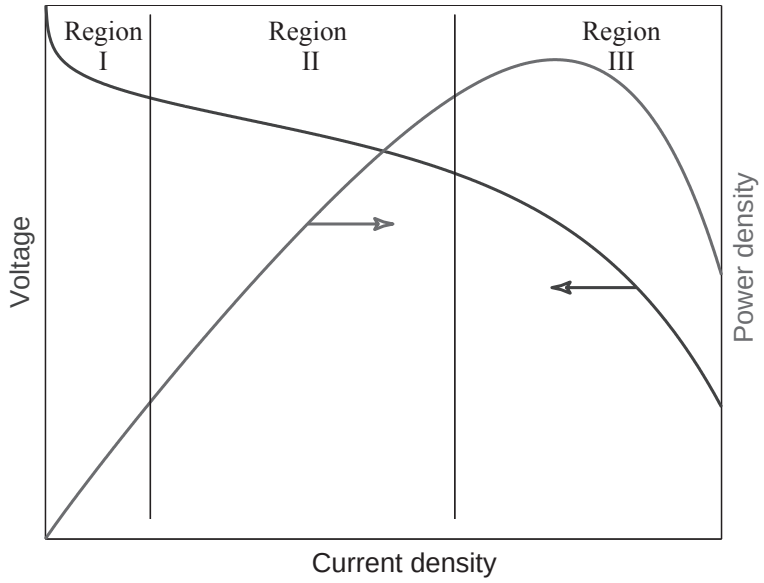

Figure 8. Current-voltage and current-power behavior of a PEFC. Region I is dominated by reaction activation, Region II by ohmic losses, and Region III by mass transfer losses.

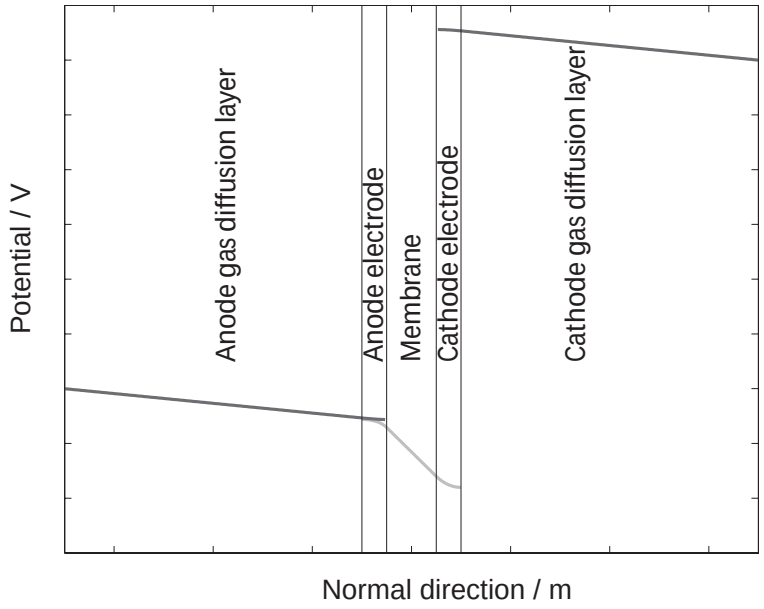

Figure 9. Typical voltage profile in a normal direction of a PEFC. (▬) refers to the electric potential, and (▬) refers to ionic potential.

2.3.3 LOSSES IN THE CATHODE ELECTRODE

The cathodic reaction, like the anodic, takes place on a platinum surface, to which oxygen, protons and electrons have to be supplied. Furthermore, product water has to be removed from the electrode in order to prevent it from blocking oxygen transfer. The transfer phenomenon in the electrode is a highly complex process involving all above-mentioned species taking part in a multi-step electrochemical reaction. It has shown that the rate determining step affecting the oxygen reduction reaction (ORR) is the first electron transfer step; see e.g. [14]. For the normal operating conditions of a PEFC, the reaction rate of the ORR can be approximated with a Tafel equation (see e.g. [13]):

$$i_{\mathrm{V}} = A i_0 \frac{c_{\mathrm{O_2}}}{c^0_{\mathrm{O_2}}} \exp\left(-\frac{\alpha_c \mathcal{F}}{\mathrm{R}T} \eta \right) \tag{6}$$

where i_{V} is the volumetric current density, A is the ratio between the real catalyst area and the geometric volume, i_0 is the exchange current per real catalyst area, c is the concentration, c^0 is the reference concentration, α_{c} is the symmetry factor for the reduction reaction, $\mathcal{F}$ is the Faraday's constant, R is the gas constant, T is the temperature and η is the overpotential. The overpotential is defined for the cathode as:

$$\eta = \phi_{\mathrm{c}} - \phi_{\mathrm{m}} - E^{\mathrm{open}} \tag{7}$$

where ϕ is the potential of the electronic (s) or ionic (m) phase and E^{open} is the open circuit potential. The Tafel equation is taken to be first-order in oxygen concentration. For a multi-step mechanism, see e.g. [14].

The electrode is nowadays assumed to be constructed of agglomerate nuclei, which in turn are structures of carbon-supported platinum and solid polymer, i.e. Nafion®. The volumetric current in this case is found from [15]:

$$i_{\mathrm{V}} = A i_0 \frac{c_{\mathrm{O_2}}}{c^0_{\mathrm{O_2}}} \left(1 - \gamma_{\mathrm{polymer}}\right)\left(1 - \gamma_{\mathrm{pores}}\right) Eff_{\mathrm{necleus}} \exp\left(-\frac{\alpha_c \mathcal{F}}{\mathrm{R}T} \eta \right) \tag{8}$$

where $\gamma_{\mathrm{polymer}}$ is the volume fraction of polymer electrolyte in the agglomerate nuclei, γ_{pores} is the volume fraction of pores in active layer and Eff_{nucleus} is the effectiveness factor of an agglomerate nucleus, i.e. a factor taking into account the oxygen diffusion into the agglomerates. The agglomerate model presented by Jaouen et al. [15] was experimentally validated in [16]. In was observed that the oxygen concentration did not radically change in the porous electrode media and thus Equation (8) can be reduced to an area-specific current density by multiplying it by the electrode height. Furthermore, if liquid water is present inside the electrode, the lost gas space has to be taken into account:

$$\mathbf{i} = Ai_0 h_{\text{electrode}} \frac{c_{\text{O}_2}}{c_{\text{O}_2}^0} (1-\gamma_{\text{polymer}})(1-\gamma_{\text{pores}})(1-s)Eff_{\text{necleus}} \exp\left(-\frac{\alpha_c \mathcal{F}}{\text{R}T}\eta\right)\mathbf{e}_{\text{n}} \quad (9)$$

where **i** is the current density with respect to the geometrical area, $h_{\text{electrode}}$ is the thickness of the electrode, s is the liquid saturation, defined as the volume occupied by liquid water divided by the volume of pores, and $\mathbf{e}_n$ is a normal vector.

In Publications A and B, cell voltage was given as a function of current density and not as in Equation (9), where current is given as a function of overpotential. However, these expressions can be derived from Equation (9) with an exception for the iR-drop. Equation (9) can be rewritten in the form:

$$\phi_{\text{c}} - \phi_{\text{m}} = E^{\text{open}} - a\ln(i) - \eta_{\text{diff}} \quad (10)$$

where η_{diff} is a function described in Publication B (Equation 3) but may also include a term for saturation as described in Equation (9). The final form is obtained when the ir-drop is included in Equation (10) giving the real cell voltage, rather than the "ir-corrected" cell voltage of Equation (10).

Overpotential in a PEFC can vary between 0 V and E^{open} and thus it affects the fuel cell efficiency significantly. Moreover, as can be seen from Equation (8) current density is a function of the overpotential and the oxygen concentration. Thus, if the concentration can be maximized more current can be drawn from the cell and the overpotential at the same current level is lower. Therefore, by maximizing the oxygen concentration at the electrode, the decrease in voltage efficiency due to the slow reaction kinetics is also reduced.

As a byproduct of the cathode reaction, a considerable amount of heat is released. The heat production at the anode side reaction is negligible because the entropy production of the reversible reaction, Equation (1), and the overpotential of the anode reaction are small compared to the corresponding terms at the cathode. The energy associated with the heat production is the difference between the total energy of the electrochemical reaction and the energy obtained as electric, and may thus be written:

$$\nabla \cdot \mathbf{q} = i_{\text{V}}\left[-\frac{\Delta H}{4\mathcal{F}} - (\phi_{\text{c}} - \phi_{\text{m}})\right] \quad (11)$$

where **q** corresponds to a heat flux. The heat production, the RHS in Equation (11), may be expanded to illustrate its different constituent terms, i.e. the reversible heat production, the open circuit heat production and the heat production due to overpotentials:

$$\nabla \cdot \mathbf{q} = i_{\mathrm{V}} \left[\underbrace{\left(\frac{-\Delta H}{4\mathcal{F}} - \frac{-\Delta G}{4\mathcal{F}} \right)}_{\text{"reversible heat"}} + \underbrace{\left(\frac{-\Delta G}{4\mathcal{F}} - E^{\text{open}} \right)}_{\text{"open circuit heat"}} + \underbrace{(-\eta)}_{\text{"overpotential heat"}} \right] \tag{12}$$

The first term in Equation (12) may also be written as the entropy production.

The heat production described by Equation (12) is valid if there are no mixed potentials due to impurities or undesirable side reactions. It has been used, e.g., by Shimpalee [34]. The mixed potentials affect both the enthalpy and the Gibbs free energy and thus no exact values can be given for these terms. Therefore, it is often assumed that the "open circuit heating" does not contribute to heat production but the "reversible heating" does, see e.g. [35-36].

The agglomerate model was used to describe the kinetics of the active layer in Publication F. In publication D, the reaction term was determined from current distribution measurements. For heat production, a determination also used by Wöhr et al. [35] and Rowe and Li [36] was used in Publication F. The model used in publication D was isothermal, and thus no heat production term was used in it.

2.3.4 MASS AND HEAT TRANSFER IN MEMBRANES

Publication D aimed to describe the cathode side mass transfer phenomena in order to reveal the limiting processes, and in Publication F, the aim was to study heat transfer in a PEFC. Because these publications did not aim to study phenomena occurring in the membrane, a constant water drag coefficient was used to describe the water transfer in both of these models and Publication F assumed constant resistance. It is, however, noted experimentally in several studies, e.g. [37-41], that the water transfer profile and resistance of the membrane can change spatially inside a working PEFC. Therefore it is important to have accurate models describing water and proton transfer.

The current membrane models using hydrodynamic approaches can be roughly divided into three groups: diffusion, hydraulic and concentrated solution models. In the diffusion model introduced by Springer et al. [42] and later used e.g. in [35, 43-48], the interaction of protons and water between sulfonic acid groups was assumed negligible. Furthermore, the model allows no pressure gradient between the anode and cathode. The water flux in the original model [42] was given as:

$$\mathbf{N}_{\mathrm{H_2O}} \cdot \mathbf{e}_{\mathrm{n}} = \frac{2.5\lambda}{11} \mathbf{i} \cdot \mathbf{e}_{\mathrm{n}} - \frac{\rho_{\mathrm{dry}}}{\mathrm{M}_{\mathrm{m}}} D_{\lambda} \frac{d\lambda}{dz} \tag{13}$$

where the contribution of migration (first factor on the RHS) and diffusion (second factor on the RHS) were determined as functions of water content λ, i.e., the ratio of the number of water molecules to the number of charge ($SO_3^-H^+$) sites, and the migration also as a function of current

density. Potential drop was calculated using an empirical formula for membrane resistance as a function of water content.

In the hydraulic model introduced by Bernardi and Verbrugge [49] and later used e.g. in [50-56], the membrane is assumed to be formed from small flow channels. In this case it is assumed that a Darcy type flow applies. In the presence of an electric field, migration is also likely to be present. Water flow is then usually modeled with the so-called Schlögl's equation [49]:

$$\mathbf{u}_{H_2O} \cdot \mathbf{e}_z = -\frac{\kappa_\phi}{\mu} c_f \mathcal{F} \frac{d\phi_m}{dz} - \frac{\kappa_p}{\mu} \frac{dp}{dz} \tag{14}$$

and the potential is obtained from

$$-\sigma_m \frac{d\phi_m}{dz} \mathbf{e}_z = \mathbf{i} - \mathcal{F} c_f \mathbf{u}_{H_2O} \tag{15}$$

where $\mathbf{u}$ is velocity, κ_ϕ is the electrokinetic permeability, κ_p is the hydraulic permeability, μ is the viscosity and c_f is the concentration of sulfonic acid groups. Rowe and Li [36] and You and Liu [57] assumed in their membrane models that water flow in the membrane is determined by diffusion, hydraulic permeation and electro-osmotic drag gained from combining the models introduced by Springer et al. [42] and Bernardi and Werbrugge [49].

A model based on the concentrated solution theory has been used by Fuller et al. [58-59] and later e.g. by Dannenberg and Lindbergh [60]. In the models based on the concentrated solution theory, the interactions between the protons, water and sulfonic acid groups are taken into account by real diffusivities. In the work by Fuller and Newman [58] and Dannenberg and Lindbergh [60], the water activity terms were assumed to be negligible for the operating conditions used in their validations. In the work by West and Fuller [59], the effect of water activity was also taken into account. Pressure was assumed to be constant or to have a negligible effect on the transfer processes.

Ise et al. [61], Janssen [62] and Vie [63] derived their expressions for transfer processes in the membrane from irreversible thermodynamics. Ise et al. [61] assumed effective diffusivity, i.e. no interaction with the sulfonic acid groups, in their analysis but included the possibility of a term describing the activity of protons as a function of molar fraction of water. In the case of Janssen the model reduces to the same expression as the model introduced by West [59].

It can be shown that all of the above-mentioned membrane models can be derived from the Maxwell-Stefan expression. In this analysis it is assumed that only water and protons are transferred inside the membrane since permeability of the membrane to gases is low [27]. The interaction between the water and protons with sulfonic acid groups is taken into account. We start from the Maxwell-Stefan equation for a case where the n:th flux corresponding to the sulfonic acid groups, is zero.

$$\mathbf{d}_{\mathrm{i}} = \sum_{\mathrm{j}=1}^{\mathrm{n}-1} \frac{x_{\mathrm{i}}\mathbf{N}_{\mathrm{j}} - x_{\mathrm{j}}\mathbf{N}_{\mathrm{i}}}{\mathrm{c_t}\mathit{Đ}_{\mathrm{ij}}} \tag{16}$$

where **d** is the driving force, x_{i} is the molar fraction of component i, $\mathbf{N}_{\mathrm{i}}$ is the molar flux of component i, c_{t} is the total concentration and $Đ_{\mathrm{ij}}$ are the Maxwell-Stefan diffusivities. The driving force for diffusion in a case where diffusion resulting from temperature gradients is negligible can be expressed as [65]:

$$c_{\mathrm{t}}\mathrm{R}T\mathbf{d}_{\mathrm{i}} = c_{\mathrm{i}}\nabla_{T,p}\mu_{\mathrm{i}} + (c_{\mathrm{i}}v_{\mathrm{i}} - \omega_{\mathrm{i}})\nabla p^{(\mathrm{l})} - \left(c_{\mathrm{i}}\mathbf{F}_{\mathrm{i}} - \omega_{\mathrm{i}}\sum_{\mathrm{j}=1}^{\mathrm{n}} c_{\mathrm{j}}\mathbf{F}_{\mathrm{j}}\right) \tag{17}$$

The electric field is the only external body force acting on species *i*, and thus can be expressed as:

$$\mathbf{F}_{\mathrm{i}} = -z_{\mathrm{i}}\mathscr{F}\nabla\phi_{\mathrm{m}} \tag{18}$$

and electroneutrality is required:

$$\sum_{\mathrm{i}=1}^{\mathrm{n}} c_{\mathrm{i}}z_{\mathrm{i}} = 0 \tag{19}$$

When the body force (18) and electroneutrality (19) are substituted in Equation (17), a general expression for the driving force in a PEFC electrolyte is obtained:

$$\mathbf{d}_{\mathrm{i}} = \frac{1}{\mathrm{R}T}\left[x_{\mathrm{i}}\nabla_{T,p}\mu_{\mathrm{i}} + \left(x_{\mathrm{i}}v_{\mathrm{i}} - \frac{\omega_{\mathrm{i}}}{c_{\mathrm{t}}}\right)\nabla p^{(\mathrm{l})} + x_{\mathrm{i}}z_{\mathrm{i}}\mathscr{F}\nabla\phi_{\mathrm{m}}\right] \tag{20}$$

In addition to electroneutrality, the conservation of mass has to apply. It is thus convenient to express Equation (16) in terms of fluxes as a function of diffusion coefficients and driving forces. By introducing diffusion term B_{ij} acting on species i–j, Equation (16) can be expressed as:

$$\mathrm{c_t}\mathbf{d}_{\mathrm{i}} = -\sum_{\mathrm{j}=1}^{\mathrm{n}-1} B_{\mathrm{ij}}\mathbf{N}_{\mathrm{i}} \tag{21}$$

where the diffusion terms are expressed as:

$$B_{\mathrm{ii}} = \sum_{\substack{\mathrm{k}=1 \\ \mathrm{i}\neq\mathrm{k}}}^{\mathrm{n}} \frac{x_{\mathrm{k}}}{Đ_{\mathrm{ik}}} \tag{22}$$

$$B_{\mathrm{ij}} = -\frac{x_{\mathrm{i}}}{Đ_{\mathrm{ij}}} \tag{23}$$

Equation (21) can be written in *n*–1 matrix form, and by taking the inverse of [*B*] one gets the formula for molar fluxes:

$$(\mathbf{N}) = -c_t [\mathbf{B}]^{-1} (\mathbf{d}) \tag{24}$$

where the inverse matrix $[B]^{-1}$ is defined as:

$$[\mathbf{B}]^{-1} = \frac{1}{|\mathbf{B}|} \begin{bmatrix} B_{22} & -B_{12} \\ -B_{21} & B_{11} \end{bmatrix} \tag{25}$$

and thus the fluxes of water and protons are:

$$\mathbf{N}_{H_2O} = -\frac{c_t}{|B|} \left(B_{22} \mathbf{d}_{H_2O} - B_{12} \mathbf{d}_{H^+} \right) \tag{26}$$

$$\mathbf{N}_{H^+} = -\frac{c_t}{|B|} \left(B_{11} \mathbf{d}_{H^+} - B_{21} \mathbf{d}_{H_2O} \right) \tag{27}$$

where

$$\mathbf{d}_{H_2O} = \left[\sum_{j=H_2O,\, H^+} \left(\delta_{H_2O,j} + x_{H_2O} \frac{\partial \ln \gamma_{H_2O}}{\partial x_j} \right) \nabla x_j \right] + \left(\frac{x_{H_2O} v_{H_2O}}{RT} - \frac{\omega_{H_2O}}{c_t RT} \right) \nabla p^{(l)} \tag{28}$$

$$\mathbf{d}_{H^+} = \left[\sum_{j=H_2O,\, H^+} \left(\delta_{H^+,j} + x_{H^+} \frac{\partial \ln \gamma_{H^+}}{\partial x_j} \right) \nabla x_j \right] + \frac{x_{H^+} \mathcal{F}}{RT} \nabla \phi_m \tag{29}$$

where $\delta_{i,j}$ is the Kronecker delta.

In Equations (28) and (29) proton concentration is assumed uniform, i.e. the morphology of the dry membrane is assumed uniform in the macroscopic scale and thus the concentration of sulfonic acid groups is uniform. Furthermore, the swelling of the membrane is assumed to have a negligible effect. Therefore, as the concentration of sulfonic acid groups is uniform, the electroneutrality forces the concentration of protons to be uniform as well. Furthermore, the effect of the pressure gradient for proton conduction is assumed negligible in Equation (29).

Current density can be calculated from Faraday's law:

$$\mathbf{i} = \mathcal{F} \sum_{i=1}^{n} z_i \mathbf{N}_i \tag{30}$$

and thus in this case, the current density simplifies to:

$$\mathbf{i} = \mathcal{F} \mathbf{N}_{H^+} \tag{31}$$

In the case of the hydraulic membrane model, the water flux was determined as velocity, which can be derived from the definition of molar flux:

$$\mathbf{u}_{\mathrm{i}} = \frac{\mathbf{N}_{\mathrm{i}}}{c_{\mathrm{t}} x_{\mathrm{i}}} \tag{32}$$

and thus the velocity of water is

$$\mathbf{u}_{\mathrm{H_2O}} = -\frac{1}{x_{\mathrm{H_2O}} |\mathbf{B}|} \left(B_{22} \mathbf{d}_{\mathrm{H_2O}} - B_{12} \mathbf{d}_{\mathrm{H^+}} \right) \tag{33}$$

The molar flux of water in the diffusion model is obtained when the activity of protons and pressure are assumed to be negligible in Equations (26)-(27), and effective diffusivity is assumed. Similarly, the hydraulic model, both Schlögl's equation and potential, is obtained when effective diffusivity is assumed and the molar fraction of water is assumed to be negligible. The models based on the concentrated solution theory are usually very similar to the model derived above but neglecting the pressure driven force.

According to Equations (26)-(29) and (31), membrane conductivity is directly proportional to the water content and pressure, and inversely proportional to temperature. It has been shown experimentally that increase in water content and in the pressure results in higher conductivity [66] but also increased temperature has been found to have an enhancing effect on conductivity [67]. Therefore, the activity and diffusion coefficients may be temperature dependent. At normal PEFC operating conditions, membrane conductivity for Nafion® membranes is around 0.15 S cm^{-1} and area specific resistance 0.1 Ω cm^2 [68]. For the voltage efficiency this means in the normal PEFC current range, approx. 0 – 10 % efficiency loss, with larger losses at elevated current densities.

The thermal conductivity of Nafion® is not well studied. Only one reference was found where the thermal conductivity of the membrane was measured [63]. Even though the measurement in the study conducted by Vie [63] was somewhat inaccurate, he could conclude that the thermal conductivity for Nafion® is 0.1 ± 0.1 W m^{-1} K^{-1}. He also noticed that the thermal conductivity is dependent on the water content but no magnitude could be estimated for that effect. Somewhat larger estimates for thermal conductivities of Nafion® have been used by Maggio et al. [69] (0.21 W m^{-1} K^{-1}) and Rowe and Li [36] (0.34 W m^{-1} K^{-1}) and for Gore PRIMEA®5510 by Hahn et al. [70] (0.25 W m^{-1} K^{-1}).

2.3.5 MASS AND HEAT TRANSFER IN GAS DIFFUSION LAYERS

Even though gas diffusion layer properties have an important role in the PEFC performance, these properties are not well characterized by experimental means. On the other hand, several studies

aiming to take into account the essential mass transfer phenomena in gas diffusion layers, among other effects, have been carried out, e.g. [14-15, 34-36, 42, 46-49, 53-60, 63, 71-85].

Most of the PEFC models assume one-phase and isothermal conditions for the PEFC, and multi-component flow in the gas diffusion layer. It has, however, been shown experimentally by Tsukada et al. [37, 86] that two-phase conditions are likely to exist under certain operating conditions. In addition, the thermal conductivity of the gas diffusion layer has recently been shown by Ihonen et al. [22] and Vie [63] to be relatively low; the effective thermal conductivity is approximately only 0.2 – 0.5 W m^{-1} K^{-1}. Therefore, both two-phase and non-isothermal conditions should be taken into account or shown to be negligible when a PEFC model is constructed.

There have been two approaches to model the two-phase flow in a PEFC; the model of Wang and Cheng [81] and that of He et al. [73]. In the model of Wang and Cheng [81], multiphase mixture parameters are calculated rather than the real flow parameters of the separated phases as it is done in the model of He et al. [73]. The model of Wang and Cheng [81] has been used later in [57, 82-83]. The model of He et al. [73] has been used later by Natarajan and Nguyen [79], in simplified form by Djilali and Lu [56], and also in Publication F.

In addition to the models by Wang and Cheng [81] and He et al. [73], Shimpalee and Dutta [80] have included the possibility for two-phase flow. However, it appears that no two-phase conditions occurred in their simulations because of the low humidification level of the inlet gases.

The difficulty of two phase flow modeling in a PEFC stems from the unknown parameters required to model the phenomena properly. Liquid flow in two-phase conditions can be expressed as the mobility of the phases and the liquid diffusion:

$$\mathbf{v}^{(\mathrm{l})} = \mathrm{m}\mathbf{v}^{(\mathrm{g})} - D^{(\mathrm{C})}\nabla s \tag{34}$$

where mobility (m) and the capillary diffusion coefficient ($D^{(\mathrm{C})}$) are expressed respectively as

$$\mathrm{m} = \frac{\kappa_{\mathrm{rel}}^{(\mathrm{l})}(s)\mu^{(\mathrm{g})}}{\kappa_{\mathrm{rel}}^{(\mathrm{g})}(s)\mu^{(\mathrm{l})}} \tag{35}$$

$$D^{(\mathrm{C})} = -\frac{\kappa\kappa_{\mathrm{rel}}^{(\mathrm{l})}(s)}{\mu^{(\mathrm{l})}}\frac{dp^{(\mathrm{C})}\left(\varphi,\theta_{\mathrm{C}},\gamma,\kappa,J(s)\right)}{ds} \tag{36}$$

where $p^{(\mathrm{C})}$ is the capillary pressure, $\kappa_{\mathrm{rel}}(s)$ are the relative permeabilities depending on saturation, φ is the surface tension, θ_{c} is the wetting angle, and $J(s)$ is the Leverett function, which also depends on saturation. The unknown parameters are those dependent on saturation, i.e. the relative permeability and the Leverett function. Functions describing these variables are usually taken from ground water flow studies, e.g. the Leverett function used by Wang and Cheng [82]. These may not describe the real characteristics of gas diffusion layers used for the PEFC, where e.g., the wetting angle is usually very high, about 150° according to Mathias et al. [87] as 0° was used in [82].

Heat transfer in PEFCs, taking into account the gas diffusion layers, has been studied in [34-36, 56, 63, 71, 80]. All of these models, apart from Djilali and Lu [56] describe flow in the gas phase only and are thus unable to take into account the cooling effect stemming from vaporization of water. It has been taken into account by Djilali and Lu [56] and the effect appears to be significant.

The thermal conductivity of the gas diffusion layer has been assumed to be relatively low throughout the heat transfer simulation studies, with the exceptions found in [56, 63]. Djilali and Lu [56] assumed that effective thermal conductivities can vary between 0.1 – 1.6 W m^{-1} K^{-1} depending on the material composition, and Vie [63] calculated effective thermal conductivities from *in-situ* PEFC measurements to vary between 0.09 – 0.23 W m^{-1} K^{-1}. Ihonen et al. [22] made *ex-situ* measurements and found similar effective thermal conductivities to Vie, varying approximately from 0.1 to 0.65 W m^{-1} K^{-1}. They also noticed that the effective thermal conductivity changed radically as a function of the clamping pressure. Similar behavior has been observed for the effective electric conductivity of similar gas diffusion layers by Mathias et al. [87] and Ihonen et al. [22]. For the electric conductivity, the bulk value was found to be independent of the clamping pressure but the interfacial conductivity changed radically [87]. Ihonen et al. [22] thus concluded that a similar level of interfacial thermal conductivity is present between the graphite current collector and the gas diffusion layers. The effect of this interfacial thermal conductivity on the PEFC temperature distribution was out of the scope of this work but is addressed in future studies [88].

When current is drawn from a PEFC, voltage losses occur also in the gas diffusion layers due to Ohmic losses resulting in decreased voltage efficiency. These losses are usually small because the area-specific resistance for the gas diffusion layers is relative high, approx. 0.01 Ω cm^2 with typical cell compressions [87], resulting in 0 – 1 % losses in voltage efficiency.

2.3.6 MASS AND HEAT TRANSFER IN CATHODE SIDE FLOW FIELD

Mass transfer in the flow fields is usually computed using the nearly incompressible Navier-Stokes equation assuming laminar flow and a multicomponent mixture for gaseous species, e.g. [34, 47-48, 71-72, 80, 84]. The possibility for two phase flow is included in [57, 82]. Heat transfer is included in models presented in [34, 71, 80]. No model capturing both heat and two-phase transfer in a gas channel exists. There is also a problem associated with the modeling of two-phase flow because the multiphase mixture model as presented in [57, 82] cannot specify in which form, i.e. droplets or film, liquid water is present in the flow field.

The inherent difference between forced and natural convection fuel cells stems from the mass transfer in the flow fields. In forced convection, velocity is generated externally with some auxiliary devices such as compressors or fans, while in free convection velocity is generated internally by buoyancy. Buoyancy forces originate from density differences, which in turn arise from temperature or concentration gradients, creating a gravitational body force [89]:

$$\mathbf{F}_{\text{buoyancy}} = \mathbf{g}\Delta\rho \tag{37}$$

where $\mathbf{g}$ is gravitation and $\Delta\rho$ is the density difference. The Navier-Stokes equation was modified by using the expression of the gravitational body force in Publication D. In Publication F, the aim was to study mass transfer in gas diffusion layers and thus channel flow was omitted from the model.

2.3.7 CURRENT DISTRIBUTION

Current distribution in a working PEFC is due to differences in reactant concentrations and in resistances of different cell components. Oxygen concentration directly affects the current production, as seen from Equation (8), and it is generally not uniform over the active area of a PEFC. This is due to the mass transfer losses in the gas diffusion layers and the finite stoichiometries and gas velocities used for the PEFC. Mass transfer can be enhanced in the gas diffusion layers e.g. by operating the cell in the one phase region, increasing the porosity and operating pressure, and minimizing the distance over which the flow must diffuse. The minimization of diffusion length should be understood to be a minimization of the width of the ribs (this favors narrow ribs and net structures) or the forced convection of flow into the gas diffusion layer, as facilitated by interdigitated flow field structures.

The concentration profiles in flow fields can be evened out by using high stoichiometries, which assure that reactants are not entirely consumed by the electrochemical reactions even at the outlet of the cell. High velocities, moreover, carry liquid water out of the cell and reduce the probability that it will block the transfer of reactants. Velocities increase with higher stoichiometries but also when the diameter of the flow channels is reduced.

The resistance of a PEFC results from the resistance of the different cell components connected electrically in series. The conductivity of the membrane depends on the concentration of water as has been observed experimentally in many studies, and can also be seen from Equations (26) – (29). However, the concentration of water is usually uneven in a working PEFC and thus the membrane conductivity can be uneven resulting in current distribution.

Spatially uneven clamping pressures may also affect current distribution because the interfacial resistances are dependent on the compression. Narrow channels and mechanically rigid structures result in more spatially uniform compression and thus also more uniform current distribution.

It is difficult to include all the necessary phenomena into a single model describing current distribution in a PEFC. Moreover, these models have to be validated against real measurement data. Therefore, different measurement techniques are needed in order to enable measurement of local phenomena, such as current, concentration, resistance, potential and temperature. The current distribution measurement techniques are discussed in the next chapter.

3 MEASUREMENT OF CURRENT DISTRIBUTION IN A PEFC

3.1 DIFFERENT MEASUREMENT TECHNIQUES

Measurement of local phenomena is important in performance and efficiency optimization of a PEFC. With whole cell measurements, only integral values of current, voltage, concentration, temperature and other cell phenomena can be observed. However, the same methods as used with whole cell measurements can be applied to local measurements, including polarization, current interruption and impedance measurements.

Local measurement techniques can be roughly divided into current distribution measurements [90-100], concentration distribution measurements [38], local probing techniques [63, 101-105] and water distribution imaging techniques [37, 40-41, 86]. Current distribution studies have been the subject of growing interest among many research groups in recent years [90-100] and particularly at HUT, see publications A-D, Reference [39], and at KTH, see Publications E-F, and the next subchapters.

A segmented PEFC should function similarly to an unsegmented one in order to ensure that real cell phenomena are observed. This means that the same current gradients should occur at given polarization. Allowances have to be, however, made in order to achieve a working segmented PEFC. These usually include inaccuracies in measurement of local current densities, uneven clamping pressures on the gas diffusion layers, and deterioration in the thermal properties of the cell.

The segment specific currents are measured in four ways in the above-mentioned articles, i.e. by using resistors [93-94, 97-98], two loads [92, 95], multi-potentiostat [90-91] or Hall sensors [99-100]. Our approach has been the use of resistors. When resistors are used to measure current, different currents drawn from the segments create different potential drops, and thus cause a different polarization for each segment. When the segments are at unequal potentials, the polarization of the electrode is changed from the real situation where the whole current collector can be expected to have same potential due to a high conductivity. However, when the IR-drop in the resistors is kept small, this does not create a significant error.

In the two load approach, all segments except of one operate with the primary load while one segment at a time is switched to secondary load. This method allows local impedance measurement, as shown by Cleghorn et al. [92]. The use of two loads does not force all segments to the same potential, and thus this method may not provide significant improvements in measurement accuracy.

Multi-potentiostatic control, involving a voltage probe for each segment, allows segment specific potential adjusting, thus giving the best accuracy. Local impedance measurements are also possible with this method [91]. Hall sensors can also be used to measure the local current. In this approach,

the cell has to be segmented in a manner similar to the other methods and the current collector material has to have relatively low electric conductivity [97].

In addition to the error caused by current probing techniques, unsegmented gas diffusion layers create additional inaccuracy to the current distribution measurements because the real active area for each segment is unknown. This is caused by current spreading in the unsegmented gas diffusion layer. However, this does not introduce a significant error to the measured values, as demonstrated by Wieser et al. [99], who concluded that the error is approx. 5 %. We also calculated an estimate for the error in Publication A and found a maximum error of approx. 15 % for a particular cell design. In that study, the in-plane conductivity was somewhat too low (380 S m^{-1} compared to an in-plane conductivity of approx. 5000 S m^{-1} measured in [87]) but on the other hand the difference between adjacent segment currents (150 mA cm^{-2}) is not likely to be as high as used in the simulation.

Segmented gas diffusion layers have been used in [92-93]. Publication E estimated the error created by the unsegmented gas diffusion. Unfortunately, the MEA was broken at the edges of each segment and therefore no reliable data could be gathered. The segmented gas diffusion layer does not, however, correspond to the real situation, as pointed out by Mench and Wang [94], because in an unsegmented PEFC current spreading already occurs in the gas diffusion layers.

Uneven clamping pressures have been noticed to create significant deviations in current distribution measurements by many groups, including ours. This is caused by the bending of the whole structure or the non-uniform resistance of the segments. Because the structures have to be rigid, they are often made quite thick, see e.g. [94, 99-100]. On the other hand, thin structures may be more usable for stack measurements [96-97]. The bigger problem, though, is usually the non-uniform resistance of the segments, which can be seen in almost all of the results published for segmented PEFCs where the distributions manifest unexpected local drops or peaks.

The free-breathing segmented PEFC, constructed at HUT, features the possibility of adjusting clamping pressure for each segment individually. This introduces another possible error source through “over adjusting” the current collectors and thus compressing the gas diffusion layers too much, resulting in lost porosity. Therefore, the adjustment can be quite laborious, taking, with bad luck, several days. One additional advantage of the adjustment system is the possibility of studying the effect of different clamping pressures on current distribution, as was conducted in Publication B.

When high current densities or PEFC stacks are studied with segmented cells, thermal conductivity for these structures has to be comparable to that for the normal current collectors. Otherwise, unrealistic heat profiles may exist throughout the cell. This in turns affects membrane conductivity and saturation conditions inside the cell. Schönbauer et al. [97] used a printed circuit board having a multilayer structure allowing sufficient thermal properties for the segmented plate. In Publication E, a structure based mainly on stainless steel for high current density applications is described. This segmented cell was constructed in order to enable stack measurements and sufficient thermal

conductivity. For a free-breathing PEFC, low thermal conductivity is not that important because of low current densities and heat production.

3.2 CURRENT DISTRIBUTION MEASUREMENT SYSTEM FOR FREE BREATHING PEFC

A current distribution measurement system, illustrated in Figure 10, was developed for a free-breathing PEFC in order to study the effect of different operating and ambient conditions on its performance. Hydrogen was used at the anode side and air transferred by natural convection from the ambient air at the cathode side. The fuel cell had a segmented current collector at the cathode side, and the segment specific currents were measured as voltage drops over high precision resistors with a data logger. The PEFC was controlled galvanostatically with a load unit, which is capable of conducting current interruption measurements.

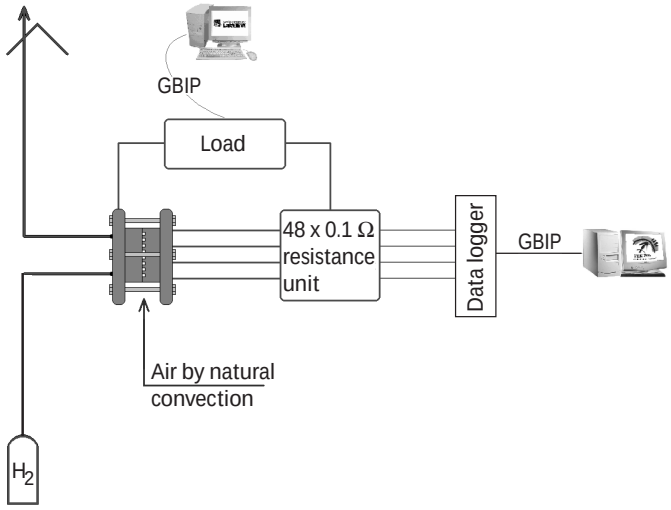

Figure 10. Measurement system.

The structure of the 5 × 5 cm segmented current collector / flow field plate is illustrated in Figure 11. Straight 3 × 3 mm channels open to the ambient air are arranged parallel to each other, with the exception of the outermost channels where the width is 1.5 mm. The current collectors forming the ribs between the channels are made of 1 mm thick and 10.5 mm wide gold-plated stainless steel plates. The plating ensures low electrical contact resistance and high chemical resistance to corrosion. A current wire is soldered onto each current collector. The matrix for the structure is made of PVC and each current collector is taped with a Teflon® coated glass fiber sheet to electrically isolate each segment from the others. The structure was stiffened with an aluminum back plate. More detailed description of the segmented plate is given in Publication A.

A special feature of this segmented plate is the possibility of individually adjusting the compression between each current collector and the gas diffusion layer. In our earlier versions of the plate, the

uneven contacts were found to result in major measurement errors, and thus they were modified to include the possibility for compression adjustments. This is achieved by two screws placed in the aluminum plate on the top of the current collector. Compression is increased by screwing down and decreased by turning back the screw. This crude method has proven to be successful for the adjustment, although it is quite laborious.

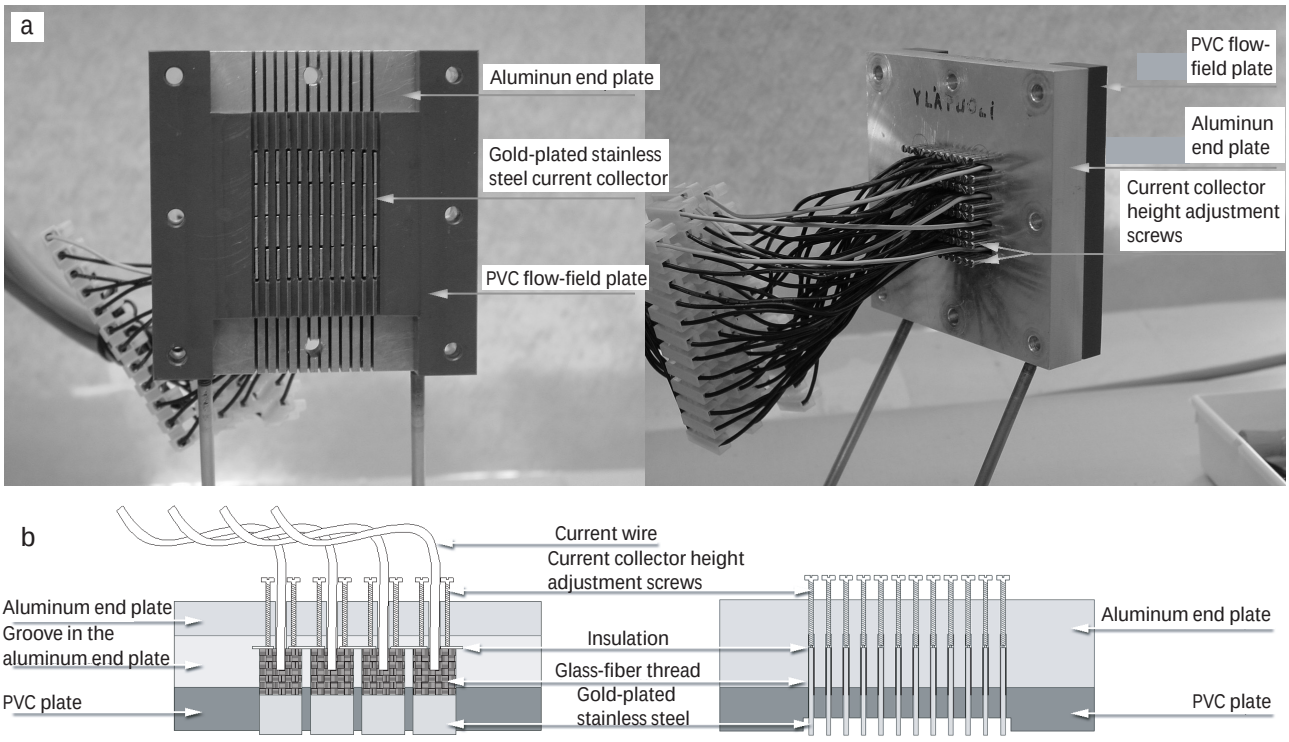

Figure 11. (a) The segmented current collector plate (left-hand side), and the end plate and the adjustment screws (right-hand side). (b) Cross-sections from the segmented cathode flow-field plate. The left one is the vertical and the right one is the horizontal cut.

Each current wire is connected through a 0.1 Ω resistor to a load. The resulting polarization between adjacent cells with 100 mA cm^{-2} difference in current density would therefore be about 5 mV. All the segments are electrically connected by the gas diffusion layer, and therefore the polarization is even minor. Furthermore, such big differences in current densities were not usual in the measurements, and thus the polarization effect should be insignificant at the low current densities where the free-breathing cell operates.

The cell concept was introduced in Publication A and measurements were conducted at different cell temperatures using pure, dry hydrogen at the anode side and ambient air at the cathode side. Exactly the same measurement system was used in Publications B and D. Current distributions were studied in more detail in Publication B where a new measurement concept was introduced to separate the contribution of different overpotentials to the current distribution. The effect of ambient conditions on the performance of the free breathing PEFC was studied in climate chamber

measurements in Publication C. The cell did require long current wires and thus current interruption measurements, used in other measurements to determine cell resistance, could not be conducted because of the impedance of the wires was too high. The longer current wires also produced additional resistance, which totaled, together with the measurement resistors, approximately 0.3 Ω for each segment.

3.3 CURRENT DISTRIBUTION MEASUREMENT SYSTEM FOR FORCED CONVECTION PEFC

A current distribution measurement system for a forced convection PEFC was constructed in order to enable studies of different flow field geometries and stack phenomena. In the first measurements reported in Publication E, two different flow field geometries were studied, both of them having a net type structure. The anode side was segmentation, whereas with the free-breathing cell the cathode side was segmented. In a free-breathing PEFC, gas tightness is not required for the cathode so it becomes considerably easier to segment. However, forced convective PEFC may be pressurized and thus gas tightness is required also for the cathode, and therefore there are no benefits to using a segmented cell at the cathode when pure hydrogen is used.

Figure 12 illustrates the cell used in the current distribution measurements, including the segmented current collector and flow field. The current collector, having active area of 90 × 60 mm, is constructed from two 3 mm thick stainless steel plates. One plate is divided into 32 segments, 8 along the flow and 4 parallel to the flow. A groove was machined behind each segment; current wires were hammered into the groove and these emerged from the edges of the segmented plate. The current collectors were placed on an unsegmented steel plate and these were electrically insulated with a thermal conductive tape. The structure was further molded into epoxy in order to ensure a leakage-proof structure. See Publication E for a more detailed description of the segmented cell structure. Otherwise the structure of the cell is the same as for the PEFC developed in the MISTRA program [106]. The same measurement system without any modifications was used in Publication F for the validation of the simulations.

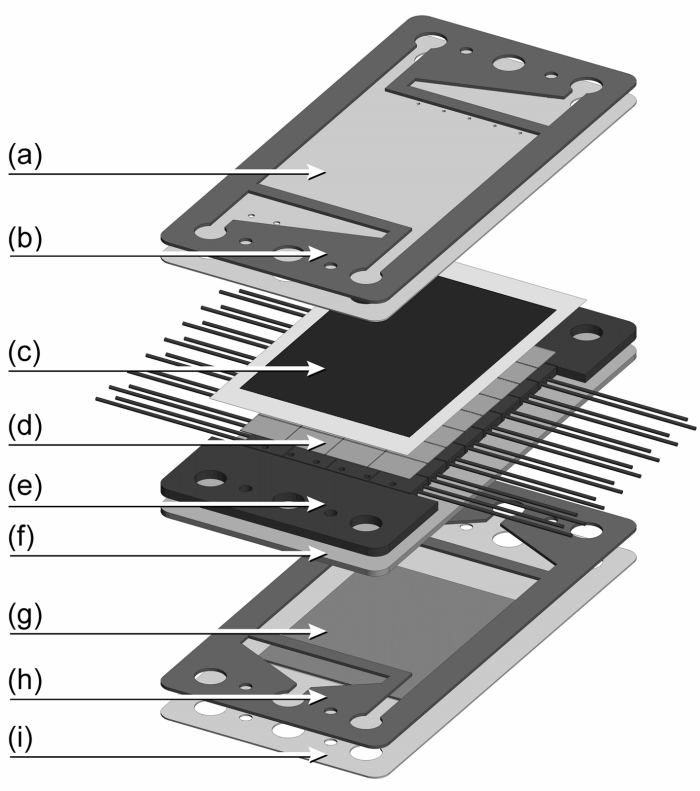

Figure 12. Structure of the segmented cell; (a) current collector; (b) gasket; (c) MEA with gas diffusion layers; (d) segmented flow field; (e) segmented current collector; (f) back-plate for the segmented current collector; (g) flow field for water; (h) gasket; (i) endplate. The anode and cathode gaskets and the flow net at the cathode side are not illustrated.

Each current wire was connected to a manual switch. One pole of the switch was connected to a terminal plate, which was further connected to a potentiostat, and the other pole was left unconnected. The switches enabled the disconnection of each individual segment from the electric circuit and thus the study of each segment individually. This was found to be a valuable diagnostic tool because malfunctioning segments could be analyzed in more detail. More reliable resistance measurements could be gained if another potentiostat were connected to system, as in [92, 95].

The segment specific currents were measured as the voltage drop between a specific point in the current wire and the terminal plate. This was found to decrease measurement accuracy because the frequent use of the manual switches had an effect on their resistances. Therefore, the measurement resistance had to be calibrated frequently. This could have been avoided by measuring the voltage drop only in the current wire. The overall resistance between a current wire and the terminal plate was approximately 10 mΩ, and thus the polarization between adjacent segments having 100 mA cm^{-2} difference in current density was only about 2 mV, resulting in negligible error in the results.

4 RESULTS

4.1 FREE BREATHING PEFC

Low airflow velocity in the cathode channels usually limits the performance of a free breathing PEFC. The flow is driven by buoyancy, which is created by thermal and concentration gradients. In a PEFC both these gradients exist because of the reactions. The temperature of a PEFC rises with increasing current due to heating by losses, and the cathode reaction consumes oxygen and produces water and thus causes concentration gradients along the gas channels.

In Publication A, the effect of the temperature gradient between the cell and ambient air was studied. The current distribution with polarization and resistance measurements were carried out at four different cell temperature levels, i.e. 30 °C, 45 °C, 60 °C and 75 °C. The ambient conditions could be treated as constant throughout the measurement series. In Publication A, the measured current distributions are shown at 100 mA cm^{-2} for all measurements and at 200 mA cm^{-2} for 45 °C and 60 °C. Here the segment specific current densities, shown in Figure 13, are averaged along the spanwise, i.e., perpendicular to the flow, direction and shown with the respective cell voltage in the form of a normal polarization curve.

One can observe from Figure 13 that an increase in the cell temperature increases the total current density up to a certain temperature level. This results from enhancement of the free convection by the increased temperature difference between the cell and ambient air. At more elevated temperatures, water produced by the cathode reaction and humidity from the ambient air are no longer sufficient to humidify the membrane and thus its resistance increases, reducing the current density.

The current distribution measurements reveal that the current production is uneven in the streamwise direction. In the spanwise direction, the distribution is relatively smooth as seen from Figures 4 – 6 in Publication A. When the resistance is not limiting the cell performance, more current is produced in the lower parts of the cell. This indicates that either the stoichiometry of the airflow is near to one or that liquid water prevents oxygen from reaching the catalyst surfaces at the top parts of the cell. Furthermore, it is interesting that the polarization curve of the two uppermost rows is bending backwards at low potentials, indicating that when current is increased, the oxygen concentration decreases more rapidly in these parts of the cell compared to the two lower segment rows. This can mean than the stoichiometry is decreased or that the amount of liquid water is increased with increased current density.

At the elevated cell temperature, i.e. 75 °C for this measurement series, the resistance of the ion conductive parts of the cell becomes the dominant loss mechanism. At this temperature, the uppermost rows produce more current than the lower ones. Hence, the polymer is likely more humid at the top parts of the cell and no severe mass transfer losses occur. However, the current distribution in the spanwise direction becomes also uneven, as seen from Figure 7 in Publication A, and thus spanwise averaging does not produce reliable data on the local cell performance.

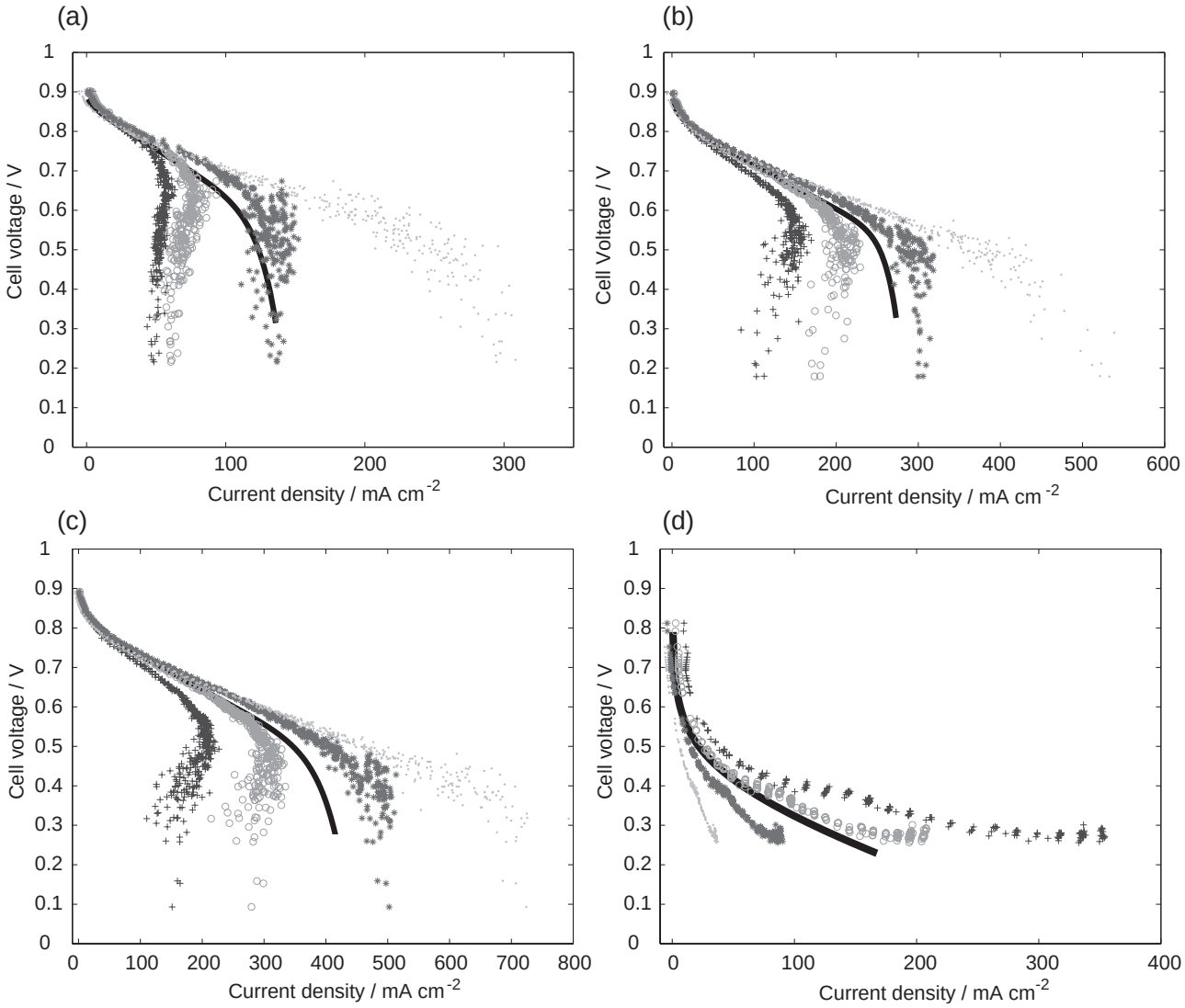

Figure 13. Effect of the temperature gradient between ambient air and the PEFC on the streamwise current distribution. The average current density is illustrated for the lowest (•), second (∗), third (o), and fourth row (+). The total current density is marked with (—). Ambient temperature was approx. 28 °C and cell temperature 30 °C (a), 45 °C (b), 60 °C (c), 75 °C (d). Relative humidity of the ambient air was approx. 50 %.

In Publication C, the effect of relative humidity on the cell performance was further studied. Fuel cell measurements were conducted with varying relative humidity levels at four different ambient temperatures. The results from the measurement conducted at an ambient temperature of 40 °C are depicted in Figure 14. The arrows in Figure 14 point from the low relative humidity conditions to the higher ones. The cell temperature was not directly controlled in the measurements but it remained relative constant, approx. 44 °C, at all humidity and current density levels. Therefore, the flow velocity and thus also the stoichiometry should have remained quite constant in the measurements.

It can again be observed that the lowest parts of the cell produce most of the current at every humidity level indicating that mass transfer in the upper parts of the cell limits the performance. The whole cell as well as the row specific cell performance decreases with increasing humidity. Even though increased humidity decreases the oxygen partial pressure and therefore some decrease in current density could be expected, the drop in performance is more than that decreased oxygen partial pressure alone could explain. The cell resistance was not measured but it is most likely that the membrane resistance did not increase with increased humidity. Therefore it is probable that the amount of liquid water in the cell is increased at higher relative humidities, explaining most of the performance losses.

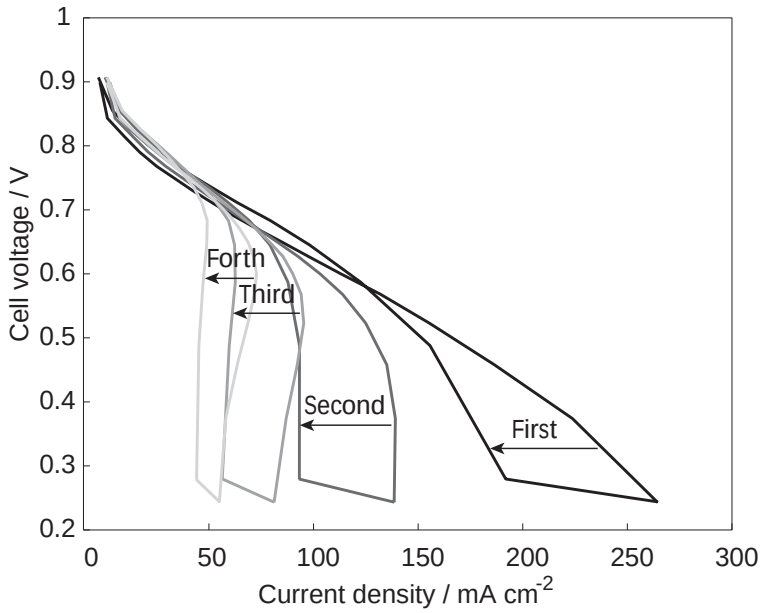

Figure 14. Effect of relative humidity of ambient air on the streamwise current distribution. The average current density is illustrated for the lowest (—), second (—), third (—), and fourth row (—). Ambient air temperature was 40 °C and relative humidity between 25 – 90 %. Cell temperature was approx. 44 °C. The arrows point from the low relative humidity condition to the high one.

The current distribution measurement system was further used in Publication B to determine the effect of different loss mechanisms on the current distribution, i.e. the uniformity of the cell resistance and oxygen concentration over the active cell area. This was achieved by measuring first the current distribution, potential and cell resistance at desirable cell conditions and then under highly over stoichiometric flow conditions. Comparing the results from these two measurements one could calculate the ohmic and mass transfer overpotential distributions by assuming that the activation overpotential was independent of the flow pulse. These distributions are shown for four different average current densities in Publication D. From these results it could be observed that the mass transfer overpotential increases in the upper parts of the cell with increasing current density.

From the mass transfer overpotential distribution one can calculate a relative oxygen concentration for each segment using Equation (3) in Publication D. It should be noted that the denominator should not be 2 but rather a constant describing the cathodic electron transfer ($\alpha_c z$), which is usually determined to be 0.5. Furthermore, Equation (3) is valid if one phase conditions occur in the electrode. If liquid water is present, it decreases oxygen transfer on the catalyst surface, which is usually treated as porosity loss. Therefore, a function that takes these modifications into account was used here:

$$\frac{c_{\mathrm{O_2,j}}}{c^0_{\mathrm{O_2}}} F(s) = \exp\left(-\frac{\alpha_c z \mathcal{F}}{\mathrm{R}T} \eta_{\mathrm{conc,j}} \right) \tag{38}$$

where $F(s)$ is a function of the liquid water saturation. The resulting distribution calculated by Equation (38), for the measurement conducted at the average current density of 180 mA cm^{-2}, is depicted in Figure 15a. The oxygen concentration is highest at the lowest segment row and decreases towards the upper parts of the cell, as expected.

As concluded in Publication B, the illustrated mass transfer overpotential distribution is likely to be somewhat smoother than the mass transfer overpotential distribution in an unsegmented PEFC due to the inaccuracies in the measurements. The same conclusion should still apply for the calculated distribution illustrated in Figure 15a. Furthermore, the cathodic electron transfer coefficient was assumed to be 0.5 whereas in Publication F it was determined to be 0.88 for the same MEA. If the later value applies then the relative concentrations should be lower and the distribution smoother.

In Publication D, a mass transfer model was created for a free breathing PEFC similar to the one used in the current distribution measurements. The model is isothermal and takes one phase, i.e. the gas phase, into account. Convection is assumed negligible in the gas diffusion layer and multicomponent flow negligible in the gas channel. Oxygen concentration is furthermore assumed uniform along the normal direction inside the electrode and along the spanwise direction in the gas diffusion layer. Thus the electrode was treated as a boundary condition and the model was two dimensional, taking the streamwise and normal directions of the cathode side of the PEFC into account. The measured current distributions were used to model the oxygen sink and water vapor source. This enabled the determination of oxygen and water vapor concentration profiles and velocities without knowing the exact kinetic parameters.

The calculation was repeated with the parameters and current distribution corresponding to the situation in Figure 15a. The resulting oxygen concentration profile along the electrode surface is illustrated in Figure 15b together with the spanwise averaged relative concentrations illustrated in Figure 15a. A polynomial of third order was, fit to the concentration profile determined with the flow pulse method, was used to extrapolate concentration profiles to the inlet and outlet regions.

The resulting concentration profiles of these two methods differ radically from each other; the flow pulse method predicts not only much lower oxygen concentrations but also a steeper decline along

the channel. Therefore it is reasonable to assume that the model used in Publication D does not include all of the essential physics needed to model a free-breathing PEFC accurately. It was shown in Publication D that the water vapor predicted by the model exceeded the maximum possible vapor pressure, conditions that occurred also with the parameters used here. Therefore, the possibility of two-phase flow should be included in the future model versions. On the other hand, the flow pulse method might not force the cathode electrode to uniform oxygen concentration, and the flow pulse might even dry the membrane resulting in differences in the conductivity. Therefore the method should be validated against real concentration measurements.

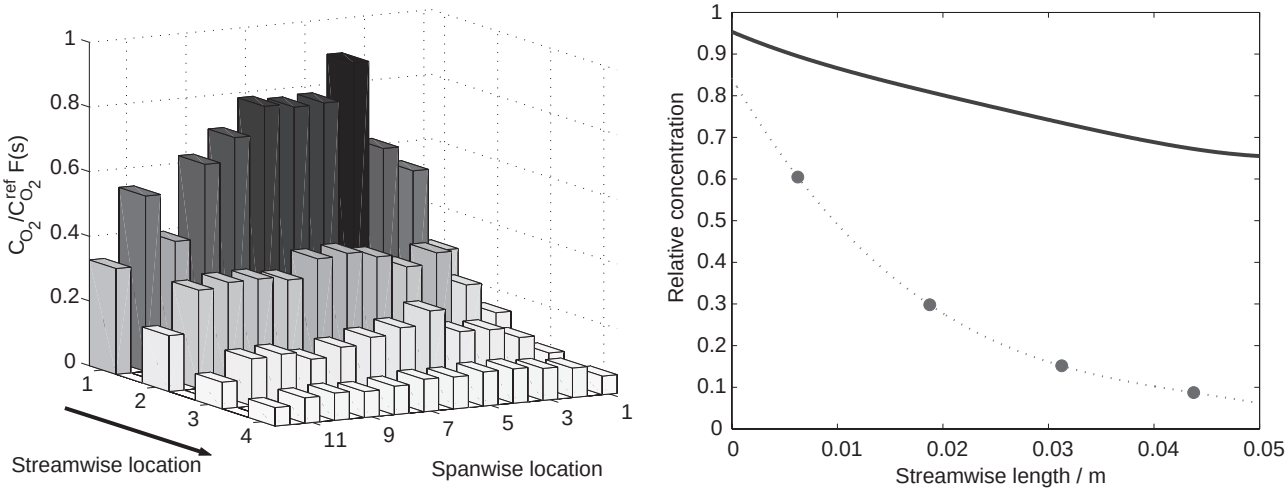

Figure 15. (a) Oxygen concentration profiles determined with the flow pulse method from measurements conducted at 180 mA cm^{-2}. The arrow points from the lower to the upper part of the channels. (b) Oxygen concentration profiles along the electrode surface determined with the model presented in Publication D (—) and with the flow pulse method presented in Publication B (- • -).

4.2 FORCED CONVECTION PEFC

Because of the losses stemming from compressing the reaction gases, PEFCs are often operated at low stoichiometries and ambient pressure. Under these conditions optimal cell design becomes increasingly important in order to prevent the formation of concentration gradients. The current distribution measurements and other local probing measurements are thus valuable tools also for such systems, too. Because the construction of these measurement systems is quite laborious, simulations are mostly used for optimization purposes. The models should, however, be validated against measured local phenomena.

A segmented current collector has been developed for net-type flow geometry and the results are used to validate a one-dimensional PEFC model. In Publication E, the use of the segmented current collector for a PEFC was demonstrated. Measurements were carried out with varying stoichiometries, oxygen partial pressures and humidity levels. Since the cathode phenomena were

under investigation, the anode inlet conditions were kept constant throughout the measurement series. In all measurements, the cell temperature was 60 °C and the cell was operated at ambient pressure.

Figure 16 illustrates the variation in the spanwise averaged current distribution as a function of the cell potential, based on measurements conducted with humidified oxygen having a dew point of 60 °C and with stoichiometric flow rate of 5.5. These conditions should produce a relative smooth current distribution profile because the high stoichiometry prevents dilution of oxygen and the high humidity avoids dehydration of the ion conductive phases. It can, however, be observed that the distribution is not uniform; the first and the last segments produce significantly less current than the other segments. This is probably due to the placement of the gas inlet and outlet holes, which create dead-zones for flow. Furthermore, segment rows 5 and 6 produce more current than the rest, probably due to the lower contact resistance of these segments. However the shape of the current distribution remains the same throughout the measured voltage range indicating that the cell conditions remain relatively constant at different polarizations.

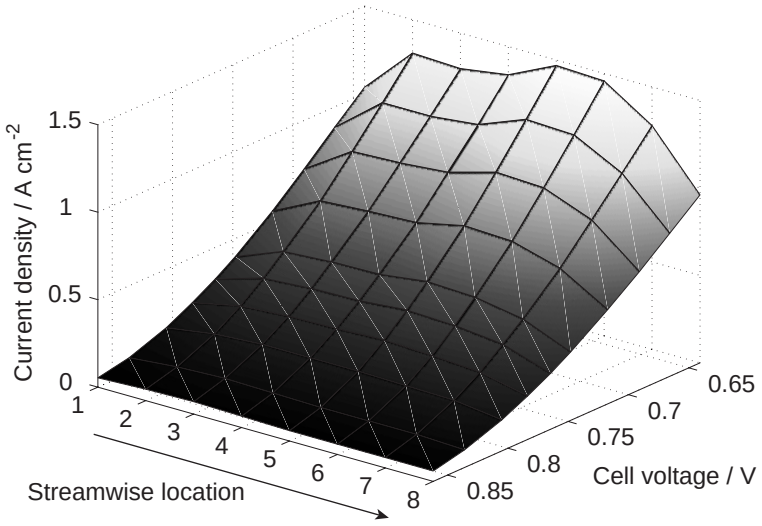

Figure 16. Spanwise averaged current distribution as a function of the cell potential. Arrow shows the flow direction for hydrogen and oxygen. The inlet dew point for hydrogen was 60 °C and the stoichiometry 3.4. The inlet dew point for oxygen was 60 °C and the stoichiometry 5.5.

It was shown in Publication B that small deviations in the segment resistances do not radically change the oxygen concentration distributions. Hence, current distributions measured at varying cell conditions can be compared to a situation in which the current distribution should be uniform. Here, current distributions were compared to the current distribution illustrated in Figure 16 and the results are depicted in Figure 17. The difference used in Figure 17 is defined as a segment current divided by the current of the same segment from the measurement conducted with oxygen having the inlet dew point at 60 °C.

Figure 17a illustrates a measurement where stoichiometry was decreased to 1.3 and air was used instead of oxygen. The increased mass transfer overpotential is obvious: more current is produced at the inlet region compared to the outlet. The increase in stoichiometry, depict in Figure 17b, decreased mass transfer limitations significantly and the observed distribution is almost identical to the one measured with oxygen. The effect of decreased humidification levels can be discerned in Figure 17c. The current production increases towards the outlet as the ion conductive phases are humidified. The differences in cell resistance and polarization between this case and the measurements conducted at higher humidity levels were, however minor, as can be seen from Figures 3 and 4 in Publication E. The combined effect of the resistance and mass transfer limitations can be observed in Figure 17d. The current density is in its maximum near the center part of the cell and the current production is limited at the inlet region by increased resistance and at the outlet region by reduced mass transfer.

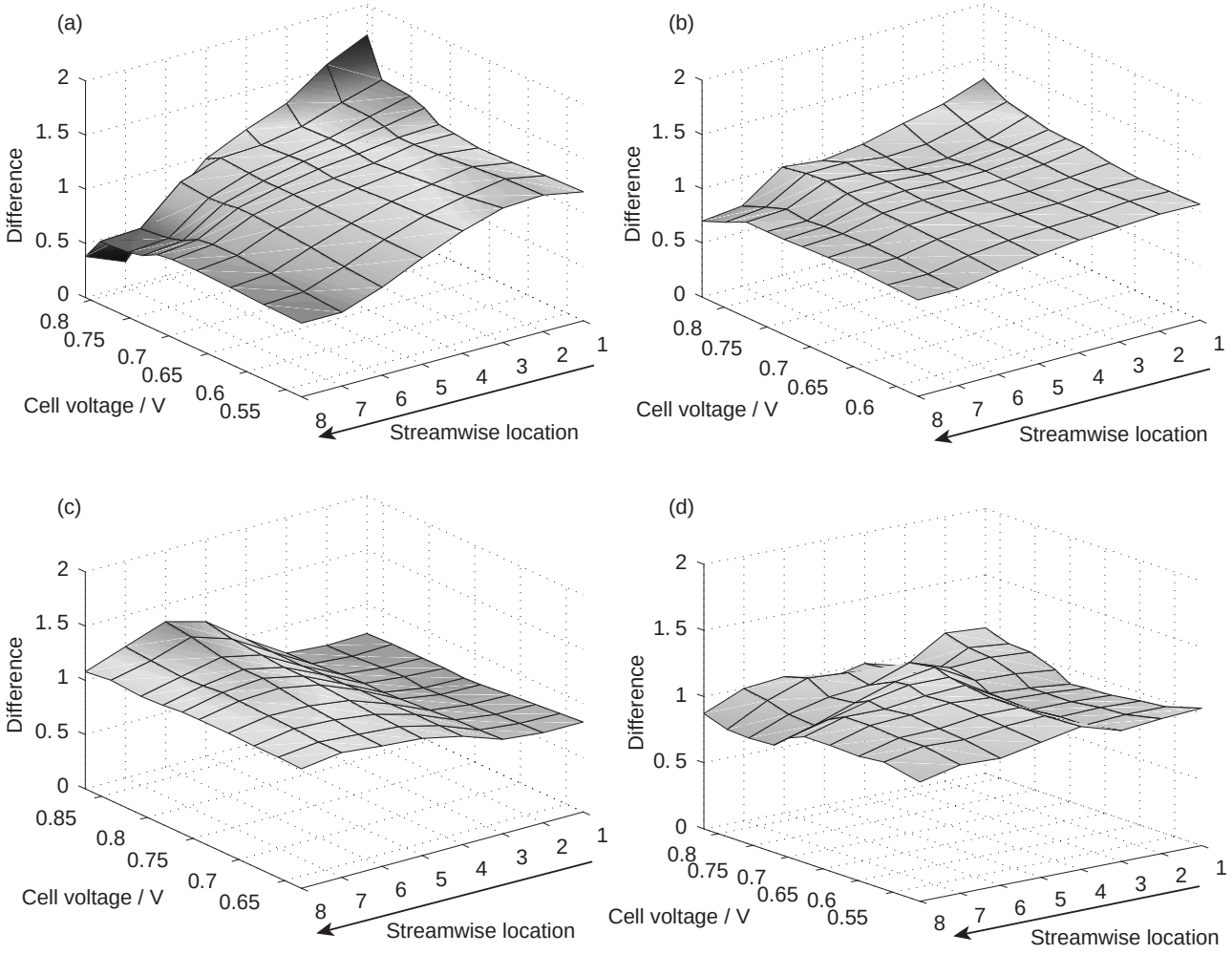

Figure 17. Spanwise averaged difference in current distributions against the cell voltage. The arrow illustrates the flow direction for hydrogen and oxygen (or air). The inlet dew point for hydrogen was 60 °C and the stoichiometry 3.4. (a) The inlet dew point for air was 60 °C and the stoichiometry 1.3; (b) the inlet dew point for air was 60 °C and the stoichiometry 2.3; (c) the inlet dew point for oxygen was 40 °C and the stoichiometry 5.5; (d) the inlet dew point for air was 40 °C and the stoichiometry 1.3.

The current distribution measurements conducted at a stoichiometry of 2.3 and a humidity level of 60 °C were used to validate a one-dimensional mass and heat transfer model of a PEFC, presented in Publication F. Because the cell used in the measurements had net-type flow geometry and the measured current distribution was relatively even, the use of a one dimensional model was justified. The modeled components were the anode and cathode side gas diffusion layers and flow fields, and the membrane.

The electrochemical reactions at the cathode side were modeled as a boundary condition with the agglomerate model by adapting the kinetic and mass transfer constants to polarization at 0.5 A cm^{-2}, resulting in a 581 mA cm^{-3} volumetric current density and a voltage slope of 30.6 V^{-1}. The conservation of charge together with Ohm's law was used to model the charge transfer throughout the modeled region. Interfacial resistances were accounted for in every interface, except the electrodes, by assuming that each had of 2.5×10^{-7} Ω m^2, estimated from [87]. The anode electrokinetics was assumed to be fast and to not affect the cell performance. At the cathode gas diffusion layer, conservation of species was taken into account in the gaseous phase with the generalized form of Fick's law and in the liquid phase by assuming that the mobility of the phases and the liquid diffusion were the main transfer mechanisms. Conservation of momentum was taken into account with Darcy's equation both for gaseous and liquid phases.

In the gas phase, oxygen, water vapor, and nitrogen were considered and in the liquid phase only water was taken into account, based on the assumption that the solubility of nitrogen and oxygen in liquid water is negligible. The phases were coupled with an interfacial water mass transfer coefficient describing the condensation / vaporization. In the model, the anode side mass transfer was assumed to be negligible. In the membrane, mass transfer was modeled with a constant water flux coefficient since no reliable data for diffusion or activation coefficients exists for the thin, Gore-Select® type membranes used in the measurements.

Heat transfer was solved for over the whole calculation domain. Convective heat flux was shown to be negligible in [88] and thus conduction was assumed to be the main transfer mechanism. The model includes ohmic heating and the heat release / sorption of the water condensation / vaporization. At the cathode electrode, heat production was assumed to result from reversible and overpotential heating but not open circuit heating, as shown in Equation (12).

Figure 18 depicts the measured and simulated polarizations. It can be seen that the normal polarization and ir-corrected polarization are predicted with high accuracy by the model at current densities over 200 mA cm^{-2}. If more accurate modeling of the low current densities is desired, then the multi-step mechanism of the cathode side reaction should be included, as discussed by Bultel et al. [14], and the Butler-Volmer equation should be used instead of the Tafel equation. Despite the small deviation between the measured and modeled polarizations at low current densities, the power density is predicted accurately throughout the current range.

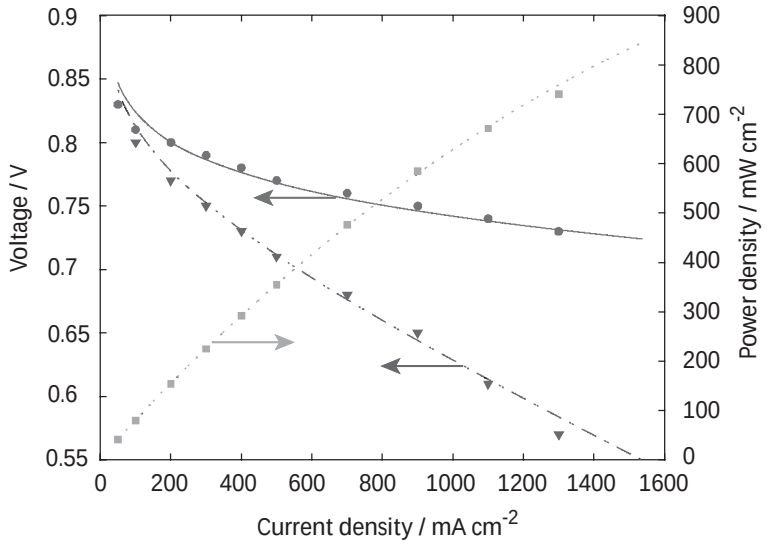

Figure 18. Measured cell polarization (▼), ir-corrected cell polarization (●) and power density (■). Modeled cell polarization (— - —), modeled ir-corrected cell polarization (—) and modeled power density (- -). For hydrogen, the inlet dew point was 60 °C and the stoichiometry 3.6, and for air the corresponding parameters were 60 °C and 2.3, respectively.

Figure 19 depicts the potential distribution through the cell at a voltage level of 0.55 V. The direction of the current is from the anode to the cathode, and thus the voltage is decreasing in the same direction with the exception of the cathode electrode, i.e. the interface between the cathode gas diffusion layer and membrane. At the cathode electrode, the oxygen reduction reaction, Equation (2), is taking place and thus increasing the voltage.

The most pronounced voltage drop occurs at the cathode electrode and is due to the slow oxygen reduction reaction. A faster oxygen reduction reaction would result in higher cathode potential; potential that is approaching the open circuit potential. Losses in the membrane are also seen to be significant but the conductivities in the solid phase are so high that their effect is shown to be minor. In this calculation, the interfacial resistances were quite small indicating high clamping pressure for the cell, and thus the voltage drop through the interfaces is small compared to the effect of the oxygen reduction reaction and the membrane resistance.

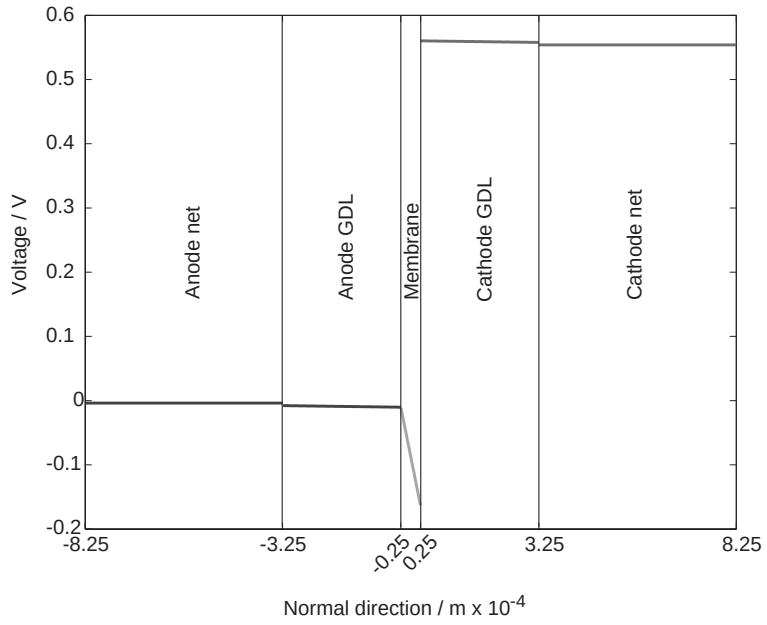

Figure 19. Potential distribution with respect to the normal cell direction calculated at a cell voltage level of 0.55 V.

The model validated in Publication F was further used here to investigate the effect of the open circuit heating and different expressions for capillary pressure. In the calculations shown in Figures 18 and 19 and in Publication F, the heat production in the cathode electrode due to the oxygen reduction reaction did not include the open circuit heating. The effect is questionable because some of the open circuit losses can be due to non-electrochemical phenomena, i.e., effects that do not contribute to the heat production, as discussed in Section 2.3.3. The expression for capillary pressure used above and in Publication F was taken from [82]. The expression has not been validated against measurements conducted with gas diffusion layers used in a PEFC and e.g. the wetting angle used in the model differs radically from the measured ones; see e.g. Mathias et al. [87]. Therefore another expression found from the literature for the dependency of the capillary pressure and saturation was used to see if these expressions predict liquid saturation differently. The expression is introduced by Natarajan et al. [79]:

$$\frac{dp^{(C)}}{ds} = -6.17\{\exp[-3.7(s-0.494)] + \exp[3.7(s-0.494)]\} \tag{39}$$

Figure 20 depicts the cell potential, ir-corrected potential and power density calculated with the base case assumptions (the model used above), with the open circuit heating included, and with the capillary pressure expression introduced by Natarajan et al. [79]. The different assumptions do not result in any major differences in the shape of the polarization curve.

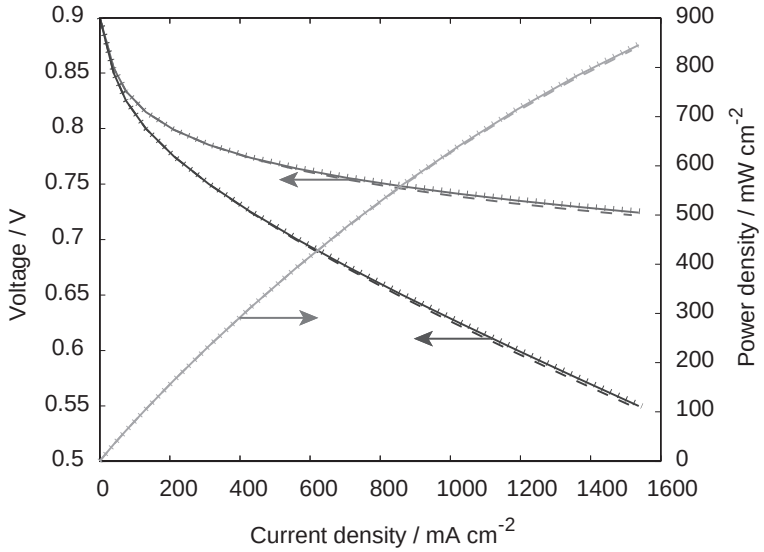

Figure 20. Modeled cell polarization (—), modeled ir-corrected polarization (—) and modeled power density (—). Wang's expression for capillary pressure (solid), Wang's expression for capillary pressure with open circuit heating included (dotted) and Natarajan's expression for capillary pressure (dashed).

When the polarization curves, illustrated in Figure 20, are studied more closely, one can observe that the cell performance is the best in the case where open circuit heating is included, and the polarization predicted using Natarajan's expression for capillary pressure results in the worst performance. The difference can be explained by the liquid water saturation depicted in Figure 21, in which (a) is again calculated with the base case, (b) with the open circuit heating included and (c) with the Natarajan's capillary pressure expression.

In the base case, the liquid water saturation on the cathode electrode ranges from 0 to 0.05, depending on the cell voltage. However, the amount of liquid water does not radically hinder the oxygen transfer into the electrode because no severe performance decrease was observed in the polarization behavior.

In the case where open circuit heating is included, less liquid water saturation is accumulated in the gas diffusion layer than in the base case. In this case, the water saturation at the cathode electrode ranges from 0 to 1.5×10^{-3} as the polarization increases. This is caused by the additional heat from the open circuit heating enabling faster evaporation of liquid water, and also increase in temperature at the cathode electrode surface as depicted in Figure 22.

The worst polarization curve was obtained with Natarajan's capillary pressure expression. Figure 21c illustrates that the highest liquid saturation levels at the cathode electrode are observed with this expression. This is a consequence of Natarajan's expression resulting in a capillary pressure about two orders of magnitude higher than that found with the expression given by Wang et al. [82] for

the same water saturation levels. The difference in saturation is, however, so small that its impact on the current distribution is almost negligible, as seen from Figure 20.

Even though there exist some *in-situ* measurements of liquid water saturation in a PEFC, none of these can be used for model validation purposes because the measurements have been conducted with completely different geometries and operating conditions. Therefore it is not possible to conclude which of the cases presented here predicts most accurately the liquid water saturation because the polarization curves predicted by the models do not differ from each other.

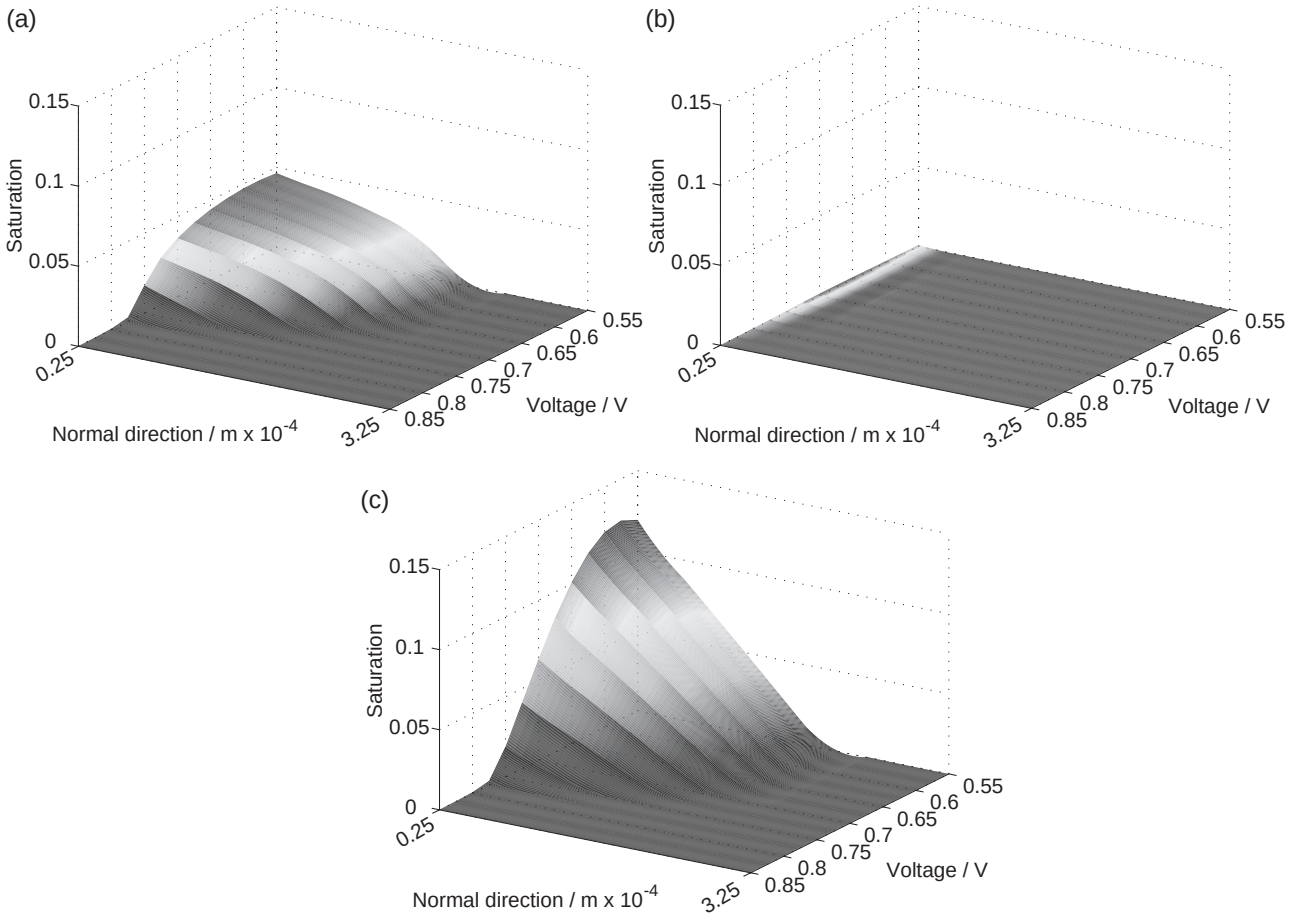

Figure 21. Liquid water saturation in the cathode side gas diffusion layer as a function of cell voltage. (a) Wang's expression for capillary pressure; (b) Wang's expression for capillary pressure with open circuit heating included; (c) Natarajan's expression for capillary pressure.

Figure 22 depicts the temperature distributions calculated with the different assumptions. In Figure 22a, the heat production of the oxygen reduction reaction was assumed to exclude the open circuit heating (base case), in Figure 22b it was included, and Natarajan's capillary pressure expression was used in Figure 22c. Effective heat conductivities were assumed in all of the cases. It should be noted that Ihonen et al. [22] observed that heat conductivity is considerable lower in the material interfaces than in the bulk. This effect was, however, excluded here.

It can be seen that the base case predicts about 55 % lower temperature differences between the cathode electrode and the cooling plate than the model including open circuit heating, but no significant difference was observed between the base case and the case where Natarajan's capillary pressure expression was used. The open circuit heating increases the heat production, and thus it is obvious that the temperature difference between the electrode and cooling plate is accordingly increased. Because the base case and the case which utilized Natarajan's capillary pressure expression predicted almost identical polarizations, the heat released in the oxygen reduction reaction was the same. Therefore, no significant differences in temperature profiles could be expected.

According to *in-situ* local temperature measurements conducted by Vie [63], the real temperature profile can be assumed to be somewhere between the base case and the case where open circuit heating was included. However, the measurement cell used by Vie had different geometry than what was used here. Whether or not the open circuit heating is included in the heat production, the model shows clearly that a PEFC operating at high current densities cannot be treated as isothermal.

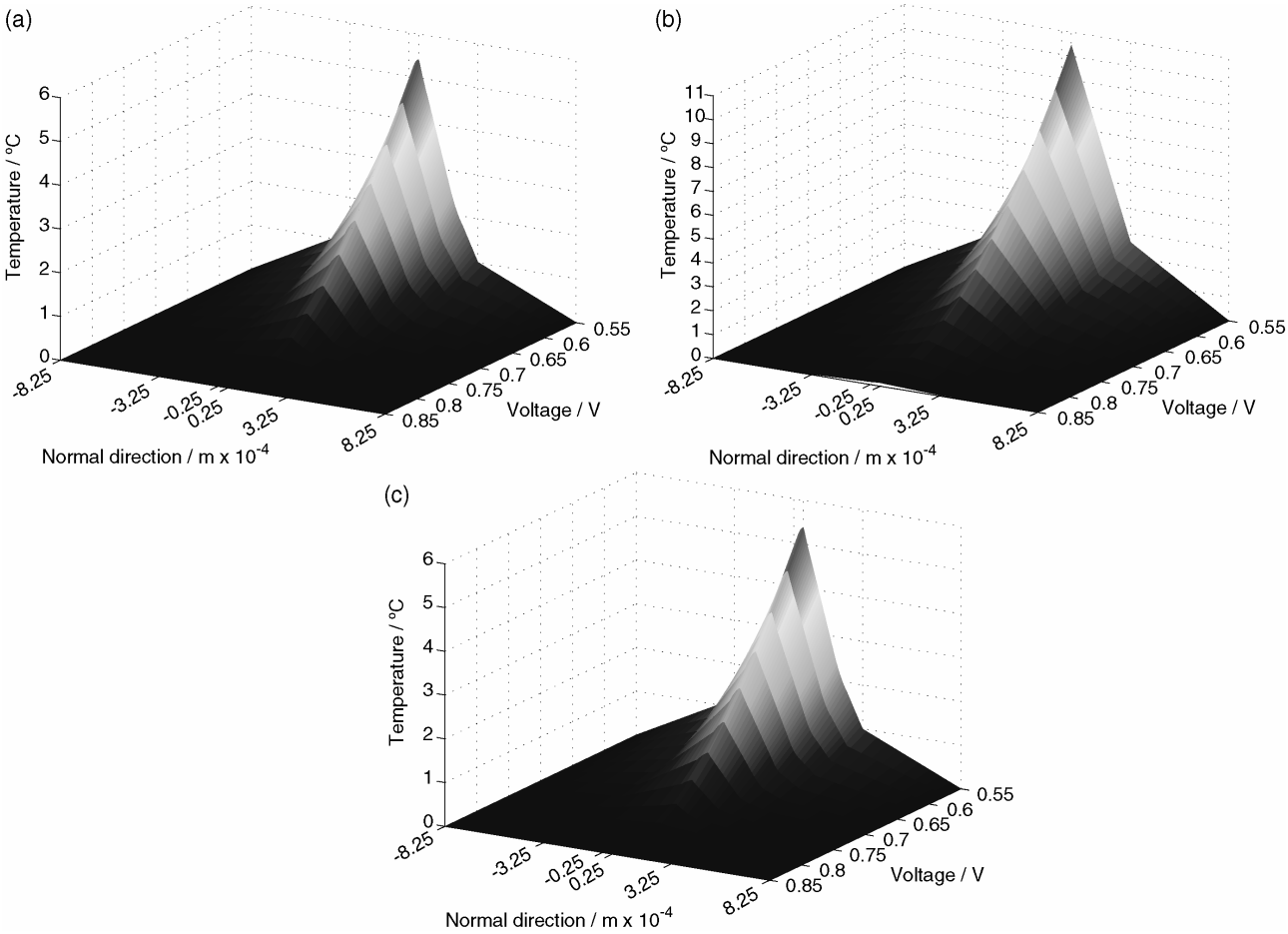

Figure 22. Temperature distribution respect to the temperature of the cooling plate in the cell as a function of cell voltage. (a) Wang's expression for capillary pressure; (b) Wang's expression for capillary pressure with open circuit heating included; (c) Natarajan's expression for capillary pressure.

5 CONCLUDING REMARKS

The single most critical factor hindering the commercialization of the PEFC systems is their cost. The cost, nowadays, is mainly determined by the amount of material used and the labor required for assembly. Therefore, it is important to use the cell area most effectively in order to reduce the material needs and thus also the costs. One important factor in the maximization of the usage of the active cell area is to ensure even current distributions at high power densities.

The current distribution in a PEFC has been studied experimentally and computationally. For experimental purposes, two different current distribution measurement systems have been constructed. These measurements make it possible to determine local current production, which in turn reveals the mass transfer characteristics for the given location. Current distribution measurements are also valuable for model validation purposes and they can be used to validate PEFC models ranging of one, two or three dimensions.

Current distribution measurements alone provide information only for the specific geometry of the measured cell. Computational approaches, however, enable studies of all kinds of geometries with small modifications. The inherent difficulty in modeling a PEFC stems from the fact that a reliable model describing the performance of a PEFC has to include many engineering disciplines. However, by combining the experimental and computational methods, more reliable models and deeper understanding of the cell behavior can be gained.

This thesis addresses small- and large-scale PEFCs. For small-scale applications, the volumetric power density of the system is often critical. Therefore, the use of passive methods to control the PEFC may be justified. Here, the use of natural convection to supply oxygen for the cathode reaction and the use of dry hydrogen were studied with a free-breathing PEFC having a segmented current collector. The use of current distribution measurements facilitated an understanding of the cell behavior going beyond the normal polarization curves used to characterize cell performance. The measurements could be used not to study not only local current production but also local membrane drying, flooding and oxygen dilution throughout the active area.

The free-breathing PEFC using non-humidified hydrogen at the anode side was studied under varying ambient conditions and at different cell temperatures. It could be observed that the cell operated well when an adequate temperature gradient, usually over 10 °C, existed between the PEFC and ambient air. However, when the cell was not actively heated, the cell performance became strongly dependent on the ambient conditions and suffered from flooding. In addition, it was observed that the cell had to be vertically orientated to allow sufficient current densities to be drawn from the cell. Some other cell geometries may be more attractive when natural convection is used, as shown e.g. by Hottinen et al. [108-109].

The current distributions from the free-breathing PEFC measurements were used for cell modeling purposes as boundary conditions. The model was used to determine the local cell phenomena that could not be directly measured, such as flow velocity and concentration distributions. The results

showed that the cell was operated at conditions were liquid water was present inside the cell. A flow-pulse method, where a highly over stoichiometric flow pulse is fed to the cell in order to smooth the oxygen concentration, was also used to study the oxygen concentrations. It could be observed that these two methods resulted in a completely different oxygen distribution profile at the electrode in the streamwise direction. Hence, the model should be upgraded to include the possibility for liquid water transfer and the flow pulse method should be validated against concentration measurements.

Current distribution was also studied in a unit cell having a net-type flow geometry capable of producing power densities up to at least 750 mW cm^{-2}. The segmented current collector was constructed in such a way as to maximize its thermal conductivity to prevent heat release from occurring only at the unsegmented side. The measurement system had, however, some problems with the segment resistances resulting in somewhat non-uniform current distributions even when pure oxygen was used. It could be shown, however, that under certain cell conditions the current production was fairly uniform and thus the results could be used to validate a one-dimensional PEFC model.

The model used to study the net-flow geometry at high stoichiometries and humidity levels included multicomponent, two-phase mass transfer at the cathode side and conservation of charge and energy throughout the modeled domain. The motivation to build such a model stems from the recent findings where it has been shown that the gas diffusion layers used in PEFCs have much lower thermal conductivities than previously expected. The results from the modeling clearly indicate that a PEFC operated at high current densities cannot be treated as isothermal but rather, several degrees of temperature differences can exist between the cathode electrode and the current collector. In addition, the cell may be simultaneously operating in two-phase conditions. It is, however, impossible to validate the liquid saturation and temperature profiles with current distribution measurements alone. Hence, local temperature and concentration measurements are needed for those purposes, together with more accurate data on the two-phase flow parameters for the gas diffusion layers and the heat production rates associated with the fuel cell reactions.

The general conclusion of this thesis, demonstrated by experimental and computational methods, is that distributed current production in a PEFC results in performance losses. These losses can be minimized by effective water management, which in turn is affected by the operating conditions, cell geometry and material properties.

REFERENCES

[1] U. Bossel, *The Birth of the Fuel Cell 1835-1845*, European Fuel Cell Forum, Oberrohrdorf, Switzerland, 2000.

[2] A. J. Appleby, F. R. Foulkes, *Fuel cell handbook*, Van Nostrand Reinhold, New York (1989).

[3] M. L. Perry, T. F. Fuller, *J. Electrochem. Soc.* **149** (2002) S59.

[4] A. Hesseldahl, "A Fuel Cell For Laptops", http://www.forbes.com/, 03.25.2002.

[5] Nafion® PFSA membranes, http://www.dupont.com/fuelcells/.

[6] W. Liu, K. Ruth, G. Rusch, *J. New. Mat. Electrochem. Systems* **4** (2001) 227.

[7] J. Wei, C. Stone, A. E. Steek, *US Patent 5,422,411* (1995).

[8] M. Rikukawa, K. Sanui, *Prog. Polym. Sci.* **25** (2000) 1463.

[9] M. Gebert, T. Grube, B. Höhlein, D. Stolten, *2nd European PEFC Forum, Proceedings,* Luzern, Switzerland (2003) 93.

[10] L. Qingfeng, H. A. Hjuler, N. J. Bjerrum, *J. Appl. Electrochem.* **31** (2001) 773.

[11] P. Jannasch, *Curr. Opin. Coll.* **8** (2003) 96.

[12] C. Boyer, S. Gamburzev, O. Velev, S. Srinivasan, A. J. Appleby, *Electrochim. Acta* **43** (1998) 3703.

[13] Y. Bultel, P. Ozil and R. Durand, *J. Appl. Electrochem.* **29** (1999) 1025.

[14] Y. Bultel, L. Genies, O. Antoine, P. Ozil, R. Durand, *J. Electroanal. Chem.* **527** (2002) 143.

[15] F. Jaouen, G. Lindbergh, G. Sundholm, *J. Electrochem. Soc.* **149** (2002) A437.

[16] J. Ihonen, F. Jaouen, G. Lindbergh, A. Lundblad, G. Sundholm, *J. Electrochem. Soc.* **149** (2002) A448.

[17] H. Wang, M. A. Sweikart, J. A. Turner, *J. Power Sources* **115** (2003) 243.

[18] J. Wind, R. Späh, W. Kaiser, G. Böhm, *J. Power Sources* **105** (2002) 256.

[19] N. Cunningham, D. Guay, J. P. Dodelet, Y. Meng, A. R. Hlil, A. S. Hay, *J. Electrochem. Soc.* **149** (2002) A905.

[20] J. Scholta, B. Rohland, V. Trapp, U. Focken, *J. Power Sources* **84** (1999) 231.

[21] T. M. Besmann, J. W. Klett, J. J. Henry, Jr., E. Lara-Curzio, *J. Electrochem. Soc.* **147** (2000) 4083.

[22] J. Ihonen, M. Mikkola, G. Lindbergh, 'The flooding of gas diffusion backing in polymer electrolyte fuel cells; physical and electrochemical characterization', Article to be submitted in J. Electrochem. Soc.

[23] J. Evertz, M. Günthart, *Proceedings of the 2nd European PEFC Forum*, Switzerland (2003) 469.

[24] E. Varkaraki, N. Lymberopoulos, A. Zachariou, *J. Power Sources* **118** (2003) 14.

[25] M. J. Lampinen, M. Fomino, *J. Electrochem. Soc.* **140** (1993) 3537.

[26] J. Koryta, J. Dvorak, L. Kavar, *Principles of Electrochemistry*, 2 ed., Wiley (1993).

[27] K. Broka (Dannenberg), P. Ekdunge, *J. Appl. Electrochem.* **27** (1997) 117.

[28] A. Parthasarathy, S. Srinivasan, A. J. Appleby, C. R. Martin, *J. Electroanal. Chem.* **339** (1992) 101.

[29] J. O'M. Bockris, S. Srinivasan, *Fuel cells, their electrochemistry*, McGraw-Hill Book Co., New York (1969).

[30] A. Damjanovic, V. Brusic, *Electrochim. Acta* **12** (1967) 615.

[31] D. B. Sepa, M. Vojnovic, L. M. Vracar, A. Damjanovic, *Electrochim. Acta* **32** (1987) 129.

[32] J. Kim, S. M. Lee, S. Srinivasan, C. E. Chamberlin, *J. Electrochem. Soc.* **142** (1995) 2670.

[33] J. Amphlett, R. Baumert, R. Mann, B. Peppley, P. Roberge, T. Harris *J. Electrochem. Soc.* **142** (1995) 1.

[34] S. Shimpalee, dissertation 'Numerical prediction of gas-humidification effects on energy transfer in PEM fuel cells', University of South Carolina, USA (2001).

[35] M. Wöhr, K. Bolwin, W. Schurnberger, M. Fischer, W. Neubrand, G. Eigenberger, *Int. J. Hydrogen Energy* **23** (1998) 213.

[36] A. Rowe, X. Li, *J. Power Sources* **102** (2001) 82.

[37] A. Tsukada, E. Lehmann, P. Vontobel, G. G. Scherer, *PSI Scientific Report 1999*, V (1999) 84.

[38] M. M. Mench, Q. L. Dong and C. Y. Wang, *J. Power Sources* (2003) in press.

[39] T. Mennola, M. Noponen, T. Kallio, M. Mikkola, T. Hottinen, *J. Appl. Electrochem.* (2003) in press.

[40] R. J. Bellows, M. Y. Lin, M. Arif, A. K. Thompson, D. Jacobson, *J. Electrochem. Soc.* **146** (1999) 1099.

[41] K. Teranishi, S. Tsushima, S. Hirai, *Thermal Science & Engineering* **10** (2002) 59.

[42] T. E. Springer, T. A. Zawodsinski, S. Gottesfeld, *J. Electrochem. Soc.* **138** (1991) 2334.

[43] T. V. Nguyen, R. E. White, *J. Electrochem. Soc.* **140** (1993) 2178.

[44] T. Okada, G. Xie, O. Gorseth, S. Kjelstrup, N. Nakamura, T. Arimura, *Electrochim. Acta* **43** (1998) 3741.

[45] P. Futerko, I-M. Hsing, *Electrochim. Acta* **45** (2000) 1741.

[46] K. Dannenberg, P. Ekdunge, G. Lindbergh, *J. Appl. Electrochem.* **30** (2000) 1377.

[47] S. Dutta, S. Shimpalee, J. W. Van Zee, *J. Appl. Electrochem.* **30** (2000) 135.

[48] S. Dutta, S. Shimpalee, J. W. Van Zee, *Int. J. Heat and Mass Transfer* **44** (2001) 2029.

[49] D. M. Bernardi, M. Verbrugge, *AIChE J.* **37** (1991) 1151.

[50] D. M. Bernardi, M. Verbrugge, *J. Electrochem. Soc.* **139** (1992) 2477.

[51] V. Gurau, H. Liu, S. Kakaç, *AIChE J.* **44** (1998) 2410.

[52] M. Eikerling, Yu. I. Kharkats, A. A. Kornyshev, Yu. M. Volfkovich, *J. Electrochem. Soc.* **145** (1998) 2684.

[53] D. Singh, D. M. Lu, N. Djilali, *Int. J. Eng. Sci.* **37** (1999) 431.

[54] S. Um, C.-Y. Wang, K. S. Chen, *J. Electrochem. Soc.* **147** (2000) 4485.

[55] G. Murgia, L. Pisani, M. Valentini, B. D'Aguanno, *J. Electrochem. Soc.* **149** (2002) A31.

[56] N. Djilali, D. Lu, *Int. J. Therm. Sci.* **41** (2002) 29.

[57] L. You, H. Liu, *Int. J. Heat and Mass Transfer* **45** (2002) 2277.

[58] T. F. Fuller, J. Newman, *J. Electrochem. Soc.* **140** (1993) 1218.

[59] A. C. West, T. F. Fuller, *J. Applied Electrochem.* **26** (1996) 557.

[60] K. Dannenberg, G. Lindbergh, Publication IV in dissertation by K. Dannenberg, '*Characterisation and Modelling of the PEMFC*', Royal Institute of Technology, Sweden (2002).

[61] M. Ise, K. D. Kreuer , J. Maier, *Solid State Ionics* **125** (1999) 213.

[62] G. J. M. Janssen, *J. Electrochem. Soc.* **148** (2001) A1313.

[63] P. J. S. Vie, Doctoral Thesis 'Characterisation and Optimisation of the Polymer Electrolyte Fuel Cell', Norges teknisk-naturvitenskapelige universitet, Norway (2002).

[64] K. Broka, P. Ekdunge, *J. Appl. Electrochem.* **27** (1997) 117.

[65] R. Taylor, R. Krishna, *Multicomponent mass transfer*, John Wiley & Sons, Inc., NY (1993).

[66] M. C. Wintersgill, J. J. Fontanella, *Electrochim. Acta* **43** (1998) 1533.

[67] M. Cappadonia, J.W. Erning, S. M. Saberi Niaki, *Solid State Ionics* **77** (1995) 65.

[68] S. Slade, S. A. Campbell, T. A. Ralph, F. C. Walsh, *J. Electrochem. Soc.* **149** (2002) A1556.

[69] G. Maggio, V. Recupero, C. Mantegazza, *J. Power Sources* **62** (1996) 167.

[70] R. Hahn, M. Krumm, H. Reichl, *19th IEEE SEMI-THERM Symposium, Proceedings*, San Jose, CA, USA (2003) 202.

[71] T. Berning, D. M. Lu, N. Djilali, *J. Power Sources* **106** (2002) 284.

[72] E. Birgersson, Licentiate Thesis 'Modelling of Transport Phenomena in Direct Methanol and Proton Exchange Membrane Fuel Cells', Royal Institute of Technology, Sweden (2003).

[73] W. He, J. S. Yi, T. V. Nguyen, *AIChE J.* **46** (2000) 2053-2064.

[74] I-M. Hsing, P. Futerko, *Chemical Engineering Science* **55** (2000) 4209.

[75] A. Kazim, H. T. Liu, P. Forges, *J. Appl. Electrochem.* **29** (1999) 1409.

[76] A. A. Kulikovsky, J. Divisek, A. A. Kornyshev, *J. Electrochem. Soc* **146** (1999) 3981.

[77] A. A. Kulikovsky, *Electrochem. Comm.* **4** (2002) 527.

[78] A. A. Kulikovsky, *Electrochem. Comm.* **4** (2002) 845.

[79] D. Natarajan, T. V. Nguyen, *J. Electrochem. Soc.* **148** (2001) A1324.

[80] S. Shimpalee, S. Dutta, *Numer. Heat Tr. A-Appl.* **38** (2000) 111.

[81] C. Y. Wang, P. Cheng, *Int. J. Heat Mass Transfer* **39** (1996) 3607.

[82] Z. H. Wang, C. Y. Wang, K. S. Chen, *J. Power Sources* **94** (2001) 40–50.

[83] L. B. Wang, N. I. Wakayama, T. Okada, *Electrochem. Comm.* **4** (2002) 584.

[84] M. Vynnycky, E. Birgersson, *SIAM J. Appl. Math.* **63** (2003) 1392.

[85] J. S. Yi, T. V. Nguyen, *J. Electrochem. Soc.* **146** (1999) 38.

[86] A. B. Geiger, A. Tsukada, E. Lehmann, P. Vontobel, G.G. Scherer, *Fuel Cells* **2** (2002) 82.

[87] M. Mathias, J. Roth, J. Fleming, W. Lehnert, *Handbook of Fuel Cells – Fundamentals, Technology and Applications, Volume 3: Fuel Cell Technology and Applications* (Eds. W. Vielstich, H.A. Gasteiger, A. Lamm) John Wiley & Sons, Ltd (2003).

[88] E. Birgersson, M. Noponen, M. Vynnycky, 'Heat Transfer Phenomena in Polymer Electrolyte Fuel Cells', Article to be submitted in J. Electrochem. Soc.

[89] F. M. White, *Viscous fluid flow, 2nd ed.*, McGraw-Hill Book Co., Singapore (1991).

[90] D. J. L. Brett, S. Atkins, N. P. Brandon, V. Vesovic, N. Vasileiadis and A. R. Kucernak, *Electrochem. Commun.* **3** (2001) 628.

[91] D. J. L. Brett, S. Atkins, N. P. Brandon, V. Vesovic, N. Vasileiadis and A. Kucernak, *Electrochemical and Solid-State Letters* **6** (2003) A63.

[92] S. J. C. Cleghorn, C. R. Derouin, M. S. Wilson and S. Gottesfeld, *J. Appl. Electrochem.* **28** (1998) 663.

[93] A. Hakenjos, K. Tüber, J. O. Schumacher, C. Hebling, *2nd European PEFC Forum, Proceedings,* Luzern, Switzerland (2003) 209.

[94] M. M. Mench, C. Y. Wang and M. Ishikawa, *J. Electrochem. Soc.* **150** (2003) A1052.

[95] N. Rajalakshmi, M. Raja and K. S. Dhathathreyan, *J. Power Sources* **112** (2002) 331.

[96] M. Santis, R. P. C. Neto, F. N. Büchi, *2nd European PEFC Forum, Proceedings,* Luzern, Switzerland (2003) 391.

[97] S. Schönbauer, T. Kaz, H. Sander, E. Gülzow, *2nd European PEFC Forum, Proceedings,* Luzern, Switzerland (2003) 231.

[98] J. Stumper, S. A. Campbell, D. P. Wilkinson, M. C. Johnson, M. Davis, *Electrochim. Acta* **43** (1998) 3773.

[99] Ch. Wieser, A. Helmbold, E. Gülzow, *J. Appl. Electrochem.* **30** (2000) 803.

[100] Y.-G. Yoon, W.-Y. Lee, T.-H. Yang, G.-G. Park, C.-S. Kim, *J. Power Sources* **118** (2003) 193.

[101] F. N. Büchi, G. G. Scherer, *PSI Scientific Report V* (1998) 57.

[102] J.-N. Han, G.-G. Park, Y.-G. Yoon, T.-H. Yang, W.-Y. Lee and C.-S. Kim, *Int. J. Hydrogen Energy* **28** (2003) 609.

[103] T. Mennola, M. Mikkola, M. Noponen, T. Hottinen, P. Lund, *J. Power Sources* **112** (2002) 261.

[104] M. Mikkola, M.Sc. Thesis 'Experimental Studies on Polymer Electrolyte Membrane Fuel Cell Stacks', Helsinki University of Technology, Finland (2001).

[105] M. Watanabe, H. Igarashi, H. Uchida, F. Hirasawa, *J. Electroanal. Chem.* **399** (1995) 239.

[106] J. Ihonen, J. Xu, S. Schwartz, A. Lundblad, G. Lindbergh, C. Kaijser, 'PEFC stack based on stainless steel net flow fields' Article to be submitted in Journal of Power Sources.

[107] S. B. Adler, *J. Electrochem. Soc.* **149** (2002) E166.

[108] T. Hottinen, M. Mikkola, T. Mennola, P. Lund, *J. Power Sources* **118** (2003) 183.

[109] T. Hottinen, M. Mikkola, P. Lund, 'Evaluation of planar free-breathing polymer electrolyte membrane fuel cell design', *J. Power Sources* (2003) Accepted for publication.

[110] M. W. Chase (ed.), *JANAF Thermochemical Tables*, 3rd Edition, Journal of physical and chemical reference data (1985).

APPENDIX A: THEORETICAL FUEL CELL OPEN CIRCUIT POTENTIAL

The Gibbs free energy (G) is a function of temperature, pressure and the reacting species. For the fuel cell reaction, the Gibbs free energy is defined as:

$$\Delta G(T,p) = \mu_{H_2O}(T,p) - \mu_{H_2}(T,p) - \frac{1}{2}\mu_{O_2}(T,p) \tag{40}$$

The chemical potential is defined as the chemical energy of a species minus the entropy produced at a given temperature and pressure:

$$\mu_i(T,p) = h_i(T,p) - Ts_i(T,p) \tag{41}$$

The temperature and pressure dependency of the chemical potential is obtained from (41) by taking the partial derivative and integrating the result from a reference temperature and pressure to the desired values:

$$\mu_i(T,p) = \Delta h_{i,0} + \int_{T_{i,0}}^{T} \frac{\partial h_i}{\partial T} dT + \int_{p_{i,0}}^{p} \frac{\partial h_i}{\partial p} dp - T\Delta s_{i,0} - T\int_{T_{i,0}}^{T} \frac{\partial s_i}{\partial T} dT - T\int_{p_{i,0}}^{p} \frac{\partial s_i}{\partial p} dp \tag{42}$$

The integrals in Equation (42) can be reduced into the following forms:

$$\Delta\mu_{i,0} = \Delta h_{i,0} - T\Delta s_{i,0} \tag{43}$$

$$\int_{T_{i,0}}^{T} \frac{\partial h_i}{\partial T} dT = \int_{T_{i,0}}^{T} C_{p,i} dT \tag{44}$$

$$T\int_{T_{i,0}}^{T} \frac{\partial s_i}{\partial T} dT = T\int_{T_{i,0}}^{T} C_{p,i} \frac{dT}{T} \tag{45}$$

$$\int_{p_{i,0}}^{p} \frac{\partial h_i}{\partial p} dp = \int_{p_{i,0}}^{p} \left[v_i - T\frac{\partial v_i}{\partial T} \right] dp \tag{46}$$

$$T\int_{p_{i,0}}^{p} \frac{\partial s_i}{\partial p} dp = -T\int_{p_{i,0}}^{p} \frac{\partial v_i}{\partial T} dp \tag{47}$$

The ideal gas law is used for the specific volumes and tabulated values from [110] are used for the specific heat capacities:

$$v_i = \frac{RT}{p} \tag{48}$$

$$C_{\mathrm{p,i}} = \sum_{\mathrm{j}=0}^{7} \mathrm{f}_{\mathrm{i,j}} T^{\mathrm{j}} \tag{49}$$

By substituting Equations (48)-(49) into Equations (44)-(47), the temperature and pressure dependencies for enthalpy and entropy are obtained:

$$\int_{T_{\mathrm{i,0}}}^{T} \frac{\partial h_{\mathrm{i}}}{\partial T} dT = \sum_{\mathrm{j}=0}^{7} \frac{\mathrm{f}_{\mathrm{i,j}}}{\mathrm{j}+1} \left(T_{\mathrm{i}}^{\mathrm{j}+1} - T_{\mathrm{i,0}}^{\mathrm{j}+1} \right) \tag{50}$$

$$T \int_{T_{\mathrm{i,0}}}^{T} \frac{\partial s_{\mathrm{i}}}{\partial T} dT = T \mathrm{f}_{\mathrm{i,0}} \ln \frac{T}{T_{\mathrm{i,0}}} + T \sum_{\mathrm{j}=1}^{7} \frac{\mathrm{f}_{\mathrm{i,j}}}{\mathrm{j}} \left(T_{\mathrm{i}}^{\mathrm{j}} - T_{\mathrm{i,0}}^{\mathrm{j}} \right) \tag{51}$$

$$\int_{p_{\mathrm{i,0}}}^{p} \frac{\partial h_{\mathrm{i}}}{\partial p} dp = 0 \tag{52}$$

$$T \int_{p_{\mathrm{i,0}}}^{p} \frac{\partial s_{\mathrm{i}}}{\partial p} dp = RT \ln \frac{p_{\mathrm{i}}}{p_{\mathrm{i,0}}} \tag{53}$$

Here the reference state for all processes is defined to be that for STP conditions. Then the chemical potential can be expressed as:

$$\begin{aligned} \mu_{\mathrm{i}}(T, p) = \Delta\mu_{\mathrm{i,0}} + \sum_{j=0}^{7} \frac{\mathrm{f}_{\mathrm{i,j}}}{\mathrm{j}+1} \left(T^{\mathrm{j}+1} - T_{\mathrm{i,0}}^{\mathrm{j}+1} \right) - \\ T \mathrm{f}_{\mathrm{i,0}} \ln \frac{T}{T_{\mathrm{i,0}}} - T \sum_{\mathrm{j}=1}^{7} \frac{\mathrm{f}_{\mathrm{i,j}}}{j} \left(T^{\mathrm{j}} - T_{\mathrm{i,0}}^{\mathrm{j}} \right) - RT \ln \frac{p_{\mathrm{i}}}{p_{\mathrm{i,0}}} \end{aligned} \tag{54}$$

The chemical potential from Equation (54) can be now inserted into Equation (40). It can be observed by comparing Equations (40) and (54) that the activity of the ideal gas is defined as the ratio of its partial pressure difference to the reference pressure. It should be noticed that it is possible that water is formed either in the liquid or gas phase, and thus one needs separate expressions to describe these situations.

If water is formed in the liquid phase, the activity of water is approximately unity and the Gibbs free energy for liquid water has to be used. If water is formed in gas phase, the activity of water is defined by its molar fraction when the reference and total pressures are identical and the Gibbs free energy for gaseous water has to be used. The formula for fuel cell theoretical open circuit potential where water is formed in liquid phase is given in Equation (55a) and for gaseous water in Equation (55b).

$$E(T,p)=\frac{1}{2\mathcal{F}}\Bigg[\Delta G_{\mathrm{high},0}+\sum_{j=0}^{7}\frac{\mathrm{f}_{\mathrm{high,j}}^{\Sigma}}{\mathrm{j}+1}\left(T^{\mathrm{j}+1}-T_0^{\mathrm{j}+1}\right)- T\mathrm{f}_0^{\Sigma}\ln\frac{T}{T_{\mathrm{i},0}}-T\sum_{\mathrm{j}=1}^{7}\frac{\mathrm{f}_{\mathrm{j}}^{\Sigma}}{\mathrm{j}}\left(T^{\mathrm{j}}-T_{\mathrm{i},0}^{\mathrm{j}}\right)-RT\ln\frac{1}{x_{\mathrm{H_2}}x_{\mathrm{O_2}}^{1/2}}\Bigg] \tag{55a}$$

$$E(T,p)=\frac{1}{2\mathcal{F}}\Bigg[\Delta G_{\mathrm{low},0}+\sum_{j=0}^{7}\frac{\mathrm{f}_{\mathrm{low,j}}^{\Sigma}}{\mathrm{j}+1}\left(T^{\mathrm{j}+1}-T_0^{\mathrm{j}+1}\right)- T\mathrm{f}_0^{\Sigma}\ln\frac{T}{T_{\mathrm{i},0}}-T\sum_{\mathrm{j}=1}^{7}\frac{\mathrm{f}_{\mathrm{j}}^{\Sigma}}{\mathrm{j}}\left(T^{\mathrm{j}}-T_{\mathrm{i},0}^{\mathrm{j}}\right)-RT\ln\frac{x_{\mathrm{H_2O}}}{x_{\mathrm{H_2}}x_{\mathrm{O_2}}^{1/2}}\Bigg] \tag{55b}$$

In Equations (55a) and (55b), the functions $\mathrm{f}_{\mathrm{j}}^{\Sigma}$ are defined as:

$$\mathrm{f}_{\mathrm{high,j}}^{\Sigma}=\mathrm{f}_{\mathrm{j},\mathrm{H_2O^{(l)}}}-\mathrm{f}_{\mathrm{j},\mathrm{H_2}}-\frac{1}{2}\mathrm{f}_{\mathrm{j},\mathrm{O_2}} \tag{56}$$

$$\mathrm{f}_{\mathrm{low,j}}^{\Sigma}=\mathrm{f}_{\mathrm{j},\mathrm{H_2O^{(g)}}}-\mathrm{f}_{\mathrm{j},\mathrm{H_2}}-\frac{1}{2}\mathrm{f}_{\mathrm{j},\mathrm{O_2}} \tag{57}$$

The switch between Equations (55a) and (55b) is defined by the maximum possible water content in the gases as:

$$\text{Equation (55a) is used if } x_{\mathrm{H_2O}}>\frac{p_{\mathrm{sat}}}{p} \tag{58a}$$

$$\text{Equation (55b) is used if } x_{\mathrm{H_2O}}\le\frac{p_{\mathrm{sat}}}{p} \tag{58b}$$

The saturation pressure is approximated by:

$$\frac{p_{\mathrm{sat}}(T)}{p}=\exp\left(28.59051-8.2\log T+0.0024804T-3142.31T^{-1}\right) \tag{59}$$

The molar fractions for oxygen, hydrogen and water are still needed. For the inlet gases, i.e. for oxygen and hydrogen, these are defined as:

$$x_{\mathrm{k}}=x_{\mathrm{k,dry}}\left(1-\frac{\Phi_{\mathrm{in}}p_{\mathrm{sat}}}{p_0}\right) \tag{60}$$

In the case of air, the molar fractions depend also on the cathode stoichiometry. The inflowing molar flux of oxygen is defined as the stoichiometric molar flux of oxygen times the excess oxygen:

$$\mathbf{n}_{\mathrm{O_2,in}} = \frac{\boldsymbol{\aleph}_{\mathrm{in}}^{(\mathrm{c})}\mathbf{I}}{4\mathcal{F}} \tag{61}$$

The inflowing molar flux of nitrogen and gaseous water can be calculated as:

$$\mathbf{n}_{\mathrm{N_2,in}} = \frac{x_{\mathrm{N_2}}}{x_{\mathrm{O_2}}}\mathbf{n}_{\mathrm{O_2,in}} = \frac{1-x_{\mathrm{O_2,dry}}}{x_{\mathrm{O_2,dry}}}\mathbf{n}_{\mathrm{O_2,in}} \tag{62}$$

$$\mathbf{n}_{\mathrm{H_2O,in}} = \frac{x_{\mathrm{H_2O}}}{x_{\mathrm{O_2}}}\mathbf{n}_{\mathrm{O_2,in}} = \frac{\boldsymbol{\Phi}_{\mathrm{in}}^{(\mathrm{c})} p_{\mathrm{sat}}}{x_{\mathrm{O_2,dry}}\left(p_0^{(\mathrm{c})} - \boldsymbol{\Phi}_{\mathrm{in}}^{(\mathrm{c})} p_{\mathrm{sat}}\right)}\mathbf{n}_{\mathrm{O_2,in}} \tag{63}$$

The total molar flux of the inlet gas stream is then the sum over all species:

$$\mathbf{n}_{\mathrm{in}} = \mathbf{n}_{\mathrm{O_2,in}} + \mathbf{n}_{\mathrm{N_2,in}} + \mathbf{n}_{\mathrm{H_2O,in}} = \frac{p_0^{(\mathrm{c})}}{x_{\mathrm{O_2,dry}}\left(p_0^{(\mathrm{c})} - \boldsymbol{\Phi}_{\mathrm{in}}^{(\mathrm{c})} p_{\mathrm{sat}}\right)}\mathbf{n}_{\mathrm{O_2,in}} \tag{64}$$

At the outlet, the molar flux of oxygen is decreased by the amount consumed in the fuel cell reaction:

$$\mathbf{n}_{\mathrm{O_2,out}} = \frac{\left(\boldsymbol{\aleph}_{\mathrm{in}}^{(\mathrm{c})} - 1\right)\mathbf{I}}{4\mathcal{F}} \tag{65}$$

The molar flux of nitrogen at the outlet is the same as at the inlet because no nitrogen is consumed in the fuel cell reaction:

$$\mathbf{n}_{\mathrm{N_2,out}} = \mathbf{n}_{\mathrm{N_2,in}} = \frac{1-x_{\mathrm{O_2,dry}}}{x_{\mathrm{O_2,dry}}}\mathbf{n}_{\mathrm{O_2,in}} \tag{66}$$

The molar flux of gaseous water is increased by the amount of water produced in the fuel cell reaction:

$$\mathbf{n}_{\mathrm{H_2O,out}} = \mathbf{n}_{\mathrm{H_2O,in}} + \frac{\mathbf{I}}{2\mathcal{F}} = \frac{\lambda\boldsymbol{\Phi}_{\mathrm{in}}^{(\mathrm{c})} p_{\mathrm{sat}} + 2x_{\mathrm{O_2,dry}}\left(p_0^{(\mathrm{c})} - \boldsymbol{\Phi}_{\mathrm{in}}^{(\mathrm{c})} p_{\mathrm{sat}}\right)}{x_{\mathrm{O_2,dry}}\left(p_0^{(\mathrm{c})} - \boldsymbol{\Phi}_{\mathrm{in}}^{(\mathrm{c})} p_{\mathrm{sat}}\right)}\frac{\mathbf{I}}{4\mathcal{F}} \tag{67}$$

The total molar flux at the outlet is also defined as the sum of all molar fluxes:

$$\mathbf{n}_{\mathrm{out}} = \mathbf{n}_{\mathrm{H_2O,out}} + \mathbf{n}_{\mathrm{N_2,out}} + \mathbf{n}_{\mathrm{O_2,out}} = \frac{\boldsymbol{\aleph}_{\mathrm{in}}^{(\mathrm{c})} p_0^{(\mathrm{c})} + x_{\mathrm{O_2,dry}}\left(p_0^{(\mathrm{c})} - \boldsymbol{\Phi}_{\mathrm{in}}^{(\mathrm{c})} p_{\mathrm{sat}}\right)}{x_{\mathrm{O_2,dry}}\left(p_0^{(\mathrm{c})} - \boldsymbol{\Phi}_{\mathrm{in}}^{(\mathrm{c})} p_{\mathrm{sat}}\right)}\frac{\mathbf{I}}{4\mathcal{F}} \tag{68}$$

Finally, the molar fraction of gaseous water is obtained from the ratio between the gaseous water molar flux and the total molar flux:

$$x_{\mathrm{H_2O}} = \frac{\mathbf{n}_{\mathrm{H_2O,out}}}{\mathbf{n}_{\mathrm{out}}} = \frac{\aleph_{\mathrm{in}}^{(\mathrm{c})} \Phi_{\mathrm{in}}^{(\mathrm{c})} p_{\mathrm{sat}} + 2x_{\mathrm{O_2,dry}} \left(p_0^{(\mathrm{c})} - \Phi_{\mathrm{in}}^{(\mathrm{c})} p_{\mathrm{sat}} \right)}{\aleph_{\mathrm{in}}^{(\mathrm{c})} p_0^{(\mathrm{c})} + x_{\mathrm{O_2,dry}} \left(p_0^{(\mathrm{c})} - \Phi_{\mathrm{in}}^{(\mathrm{c})} p_{\mathrm{sat}} \right)} \tag{69}$$

APPENDIX B: THEORETICAL FUEL CELL EFFICIENCY

The efficiency is defined as the ratio between the energy obtained from a process and the energy put into the process. In the case of a fuel cell, the theoretical maximum electric energy obtained from the fuel cell reaction is the Gibbs free energy and the total energy is the enthalpy.

$$\eta_{\text{theoretical}} = \frac{\Delta G(T,p)}{\Delta H(T,p)} \tag{70}$$

The Gibbs free energy can be calculated from Equations (40) and (54) and enthalpy can be found from:

$$\Delta H(T,p) = h_{\text{H}_2\text{O}}(T,p) - h_{\text{H}_2}(T,p) - \frac{1}{2} h_{\text{O}_2}(T,p) \tag{71}$$

The temperature and pressure dependencies are obtained as:

$$h_{\text{i}} = h_{\text{i,0}} + \int_{T_{\text{i,0}}}^{T} \frac{\partial h_{\text{i}}}{\partial T} dT + \int_{p_{\text{i,0}}}^{p} \frac{\partial h_{\text{i}}}{\partial p} dp \tag{72}$$

The reaction enthalpy is then obtained by substituting Equations (44), (46) and (72) into Equation (71). It should be again noted that water can be formed in the liquid and gaseous phases and thus two different formulas are needed for enthalpy:

$$\Delta H(T,p) = \Delta H_{\text{high,0}} + \sum_{\text{j=0}}^{7} \frac{\text{f}_{\text{high,j}}^{\Sigma}}{\text{j}+1} \left(T^{\text{j}+1} - T_0^{\text{j}+1} \right) \tag{73a}$$

$$\Delta H(T,p) = \Delta H_{\text{low,0}} + \sum_{\text{j=0}}^{7} \frac{\text{f}_{\text{low,j}}^{\Sigma}}{\text{j}+1} \left(T^{\text{j}+1} - T_0^{\text{j}+1} \right) \tag{73b}$$

The switch between Equations (73a) and (73b) is defined by Equations (58a) and (58b).